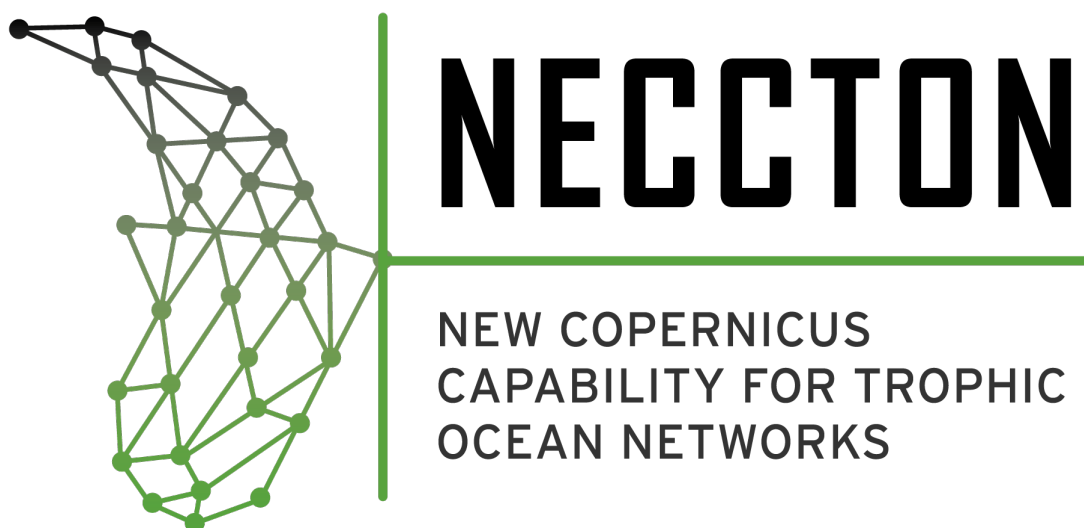


<b>Project</b>	NECCTON No 101081273	<b>Start / Duration</b>	2023-2026
<b>Dissemination</b>	Public	<b>Nature</b>	Report
<b>Date</b>	31 <sup>st</sup> December 2024	<b>Version</b>	1.0



## Deliverable 4.2

### Assessment of L2 PRISMA production chain, outputs and transferability

<b>Deliverable Contributors:</b>	<b>Name</b>	<b>Organisation</b>	<b>Role / Title</b>
<b>Deliverable Leader</b>	Federica Braga	CNR	Task Leader
<b>Contributing Author(s)</b>	Giuliana Profeti	CNR	WP4 contributor
	Paolo Lazzari	OGS	WP4 contributor
	Eva Álvarez	IEO-CSIC	WP4 contributor
	Gian Marco Scarpa	CNR	WP4 contributor
	Giorgia Manfè	CNR	WP4 contributor
	Luis Gonzalez Vilas	CNR	WP4 contributor
	Jozef Skakala	PML	WP4 contributor
	Vittorio Brando	CNR	WP4 contributor
<b>Reviewer(s)</b>	Jozef Skakala	PML	Internal Reviewer
	Claudia Giardino	CNR	External Reviewer
<b>Final review and approval</b>	Stefano Ciavatta	MOi	Project lead



<b>Project</b>	NECCTON No 101081273	<b>Deliverable</b>	4.2
<b>Dissemination</b>	Public	<b>Nature</b>	Report
<b>Date</b>	31 <sup>st</sup> December 2024	<b>Version</b>	1.0

#### Document History:

Release	Date	Reason for Change	Status	Distribution
0.0	09/12/2024	Initial document, to be reviewed	Released	Internal
1.0	31/12/2024	Final revised report	Released	Public

#### To cite this document

Braga, F., Profeti, G., Lazzari, P., Álvarez, E., Marco Scarpa, G., Manfè, G., Gonzalez Vilas, L., Skakala, J., & Brando, V. (2024). NECCTON D4.2 Assessment of L2 PRISMA production chain, outputs and transferability. DOI Zenodo. [10.5281/zenodo.14551764](https://doi.org/10.5281/zenodo.14551764)

<b>Project</b>	NECCTON No 101081273	<b>Deliverable</b>	4.2
<b>Dissemination</b>	Public	<b>Nature</b>	Report
<b>Date</b>	31 <sup>st</sup> December 2024	<b>Version</b>	1.0

## TABLE OF CONTENTS

1.	Executive Summary .....	4
2.	Scope .....	5
2.1	Definitions and Acronyms .....	5
3.	Introduction .....	6
3.1	Imaging spectrometry .....	6
4.	Study sites.....	8
4.1	Acqua Alta Oceanographic Tower.....	9
4.2	Casablanca Platform .....	9
4.3	Galata Platform and Section-7 Platform.....	9
4.4	Boussole Buoy.....	9
4.5	L4 Scientific Buoy .....	10
5.	Data.....	10
5.1	<i>In situ</i> radiometric data .....	10
5.1.1	AERONET-OC network.....	10
5.1.2	WATERHYPERNET network .....	11
5.2	PRISMA hyperspectral imagery .....	12
5.2.1	Standard PRISMA products .....	13
5.2.2	PRISMA dataset for the present study.....	14
6.	Methodology.....	15
6.1	Atmospheric correction processors .....	15
6.1.1	Standard L2C processor .....	15
6.1.2	ACOLITE .....	16
6.1.3	POLYMER.....	17
6.2	Match-up analysis.....	17
7.	Results .....	20
7.1	Qualitative analysis.....	20
7.2	Quantitative analysis.....	32
8.	Transferability of the validation approach to future hyperspectral missions.....	41
9.	PRISMA data stream as validation and assimilation tool for biogeochemical models .....	43
10.	Acknowledgments .....	45
11.	References.....	46

<b>Project</b>	NECCTON No 101081273	<b>Deliverable</b>	4.2
<b>Dissemination</b>	Public	<b>Nature</b>	Report
<b>Date</b>	31 <sup>st</sup> December 2024	<b>Version</b>	1.0

## 1. Executive Summary

Spaceborne imaging spectrometry provides measurements across numerous discrete narrow bands, forming a contiguous spectrum that enables the retrieval of key biogeophysical parameters in aquatic ecosystems, such as the characterization of phytoplankton, dissolved and suspended matter and other optically active biological constituents. One of the objectives of NECCTON is to provide Copernicus Marine Service (CMEMS) with new capability in fusing numerical model simulations and novel satellite observations, including new hyperspectral observations from the PRISMA satellite mission. Multiple biogeochemical models will be upgraded by adding bio-optical modules describing the distribution of in-water irradiance along the water column and the interaction of optically active substances with the spectral light field. The integration of hyperspectral imagery and biogeochemical models by means of augmented skill-performance metrics and novel assimilation techniques is a challenging application for improving model parameters and enhancing the description of plankton and optically active properties. A prerequisite for model validation and a successful data assimilation is an accurate estimation of uncertainties in the satellite observations. To this end, we explored the potential and limitations of PRISMA hyperspectral mission to provide water reflectance products in coastal and marine sites, where PRISMA data are still underexploited.

In this document, we present the assessment of Standard PRISMA Level 2 (L2) products, distributed by the Italian Space Agency (ASI), and data derived from two atmospheric correction (AC) processors, ACOLITE and POLYMER, adapted for processing PRISMA Level 1 (L1) products, using *in situ* reflectance from autonomous multispectral and hyperspectral radiometer systems, such as AERONET-OC and WATERHYPERNET. We analysed a total of 79 PRISMA images, acquired from July 2019 to March 2024 over six sites: Acqua Alta Oceanographic Tower (AAOT) in the Northern Adriatic Sea, Galata and Section-7 Platform in the Black Sea, Casablanca Platform in the Western Mediterranean Sea, Boussole Buoy in the Ligurian Sea and L4 Scientific Buoy in the Western English Channel.

The qualitative and quantitative analyses of Remote Sensing Reflectance (Rrs) derived from PRISMA L2 and PRISMA L1 corrected with ACOLITE and POLYMER were performed in the four sites, where *in situ* radiometric data from AERONET-OC network were available. Overall, the deviation of L2 with respect to *in situ* data was high on some dates, while Rrs derived from POLYMER matched quite well. The performances of the AC processors were statistically estimated at the nine AERONET-OC bands in the 412 – 667 nm range, confirming that the standard PRISMA L2 product had the weaker performances in marine and coastal waters. POLYMER gave the best results among the four sites with a good correlation with AERONET-OC measurements in the 443 - 560 nm spectral range. The ACOLITE product was characterized by an overall overestimation of the reflectance spectrum, with improved results when the glint correction was applied. In general, all the processors produced data affected by systematic overestimations, however, the results are encouraging, confirming the consistency of PRISMA Rrs and its capability in providing adequate radiometric products. The availability of Rrs data from autonomous systems is fundamental to provide validation data and thoroughly assess the radiometric performance of PRISMA Rrs between 400 and 900 nm.

<b>Project</b>	NECCTON No 101081273	<b>Deliverable</b>	4.2
<b>Dissemination</b>	Public	<b>Nature</b>	Report
<b>Date</b>	31 <sup>st</sup> December 2024	<b>Version</b>	1.0

First “very preliminary” results on NASA’s PACE, the novel hyperspectral mission launched on February 2024, compared with *in situ* hyperspectral data from WATERHYPERNET network at AAOT, are also presented to test the transferability of the validation approach. Moreover, for the AAOT site in the Adriatic Sea, we performed a preliminary comparative analysis of Rrs spectra derived from the GOTM-FABM-BFM bio-optical biogeochemical model and observations from OLCI/Sentinel-3 and PRISMA data processed with POLYMER and ACOLITE.

## 2. Scope

This document shows the results of the qualitative and quantitative comparison of PRISMA Rrs spectra, obtained from three AC processors versus *in situ* data over selected NECCTON sites. The assessment of the performance of PRISMA L2 products is a prerequisite for model validation and data assimilation in bio-optical biogeochemical models, developed by NECCTON partners.

### 2.1 Definitions and Acronyms

AAOT	Acqua Alta Oceanographic Tower
AC	Atmospheric correction
AERONET	Aerosol Robotic Network
AERONET-OC	Aerosol Robotic Network-Ocean Colour
AOT	Aerosol Optical Thickness
ASI	Italian Space Agency
BOA	Bottom-of-Atmosphere
Boussole	BOUée pour l'acquiSition d'une Série Optique à Long termE
BRDF	Bidirectional reflectance distribution function
CHIME	Copernicus Hyperspectral Imaging Mission for the Environment
CMEMS	Copernicus Marine Service
DDV	Dense Dark Vegetation
DSF	Dark Spectrum Fitting
$E_d$	Downwelling Irradiance
EnMAP	Environmental Mapping and Analysis Program
ESA	European Space Agency
$F_0$	mean extraterrestrial solar irradiance
FWHM	Full Width at Half Maximum
GC	Glint Correction
GSD	Ground Sampling Distance
HDF-EOS5	Hierarchical Data Format - Earth Observing System
HYPSTAR	HYperspectral Pointable System for Terrestrial and Aquatic Radiometry
ISS	International Space Station
L1	Level 1
L2	Level 2
$L_d$	downwelling radiance
$L_{TOA}$	Top-Of-Atmosphere radiance

<b>Project</b>	NECCON No 101081273	<b>Deliverable</b>	4.2
<b>Dissemination</b>	Public	<b>Nature</b>	Report
<b>Date</b>	31 <sup>st</sup> December 2024	<b>Version</b>	1.0

LUT	Look-Up Table
$L_{wn}$	Water-leaving radiances
$L_{wn}$	Normalised water-leaving radiances
MAD	Mean Absolute Difference
MAPD	Mean Absolute Percentage Difference
MFC	Monitoring and Forecasting Centre
NASA	National Aeronautics and Space Administration
NECCON	New Copernicus capability for trophic ocean networks
OCI	Ocean Color Instrument
OLCI	Ocean and Land Colour Instrument
OSOAA	Ordres Successifs Océan Atmosphère
PACE	Plankton, Aerosol, Cloud, ocean Ecosystem
PAN	panchromatic
PANTHYR	Pan-And-Tilt HYperspectral Radiometer
PAR	Photosynthetically available radiation
PRISMA	PRecursore IperSpettrale della Missione Applicativa
RMSD	Root Mean Square Difference
ROI	Region of Interest
$R_{rs}$	Remote sensing reflectance
SA	Spectral Angle
SBG	Surface Biology and Geology
SeaPRISM	Photometer Revision for Incident Surface Measurements
SeaWiFS	Sea-Viewing Wide Field-of-View Sensor
SNR	Signal-to-Noise Ratio
SSI	Spectral Sampling Interval
SWIR	Short-Wave Infrared
SZA	Solar Zenith Angle
TOA	Top-Of-Atmosphere
VNIR	Visible to Near InfraRed
WV	Water Vapor columnar content

## 3. Introduction

### 3.1 Imaging spectrometry

Traditional ocean colour satellite missions involve multispectral sensors with a limited number of broad and discontinuous bands in the visible and infrared spectral range mainly designed to detect the concentration of the primary pigment in phytoplankton, chlorophyll-a (Gordon and Morel, 1983). In the last few decades, earth observation has advanced rapidly including imaging spectrometers, which provide measurements in many narrow and spectrally contiguous bands, retrieving a continuous spectrum that can represent biogeophysical parameters and processes

<b>Project</b>	NECCTON No 101081273	<b>Deliverable</b>	4.2
<b>Dissemination</b>	Public	<b>Nature</b>	Report
<b>Date</b>	31 <sup>st</sup> December 2024	<b>Version</b>	1.0

(Goetz et al., 1985). Inspired by the achievements of airborne hyperspectral imagery and growing user demand, spaceborne hyperspectral sensors have taken a step forward with advances in payload technology, sensor performance and on-board calibration equipment (Transon et al., 2018; Rast and Painter, 2019; Giardino et al., 2019; Dierssen et al., 2021).

In the first decade of the new millennium, spaceborne imaging spectrometers were launched as technology demonstration missions. These hyperspectral missions were the main sources of hyperspectral satellite data for years, but the amount and the quality of data were quite insufficient for a wide range of potential applications (Guanter et al., 2015). In recent years, several national hyperspectral missions have been launched, including the German DESIS, onboard the International Space Station (ISS), China's AHSI, aboard the GaoFen-5 satellite and HyperScout-1, a smart hyperspectral imager for nanosatellites, all launched in 2018; the Japanese HISUI and the Italian PRISMA, which were launched in 2019; the German EnMAP, launched in 2022 and the NASA's PACE, launched on February 2024.

Although the capabilities of spaceborne imaging spectrometry in aquatic environments have been demonstrated in several case studies, there are crucial issues that remain unresolved in comparison to data from multispectral satellites, such as i) the availability of *in situ* hyperspectral fiducial reference measurements, ii) atmospheric correction, including the air–water interface effects; and iii) signal-to-noise ratio and the overall sensitivity of water reflectance (Braga et al., 2022). The aforementioned challenges should be addressed in order to adequately prepare for forthcoming operational spaceborne hyperspectral missions. ESA and NASA have identified hyperspectral missions as crucial for addressing significant scientific and environmental management objectives. Two notable examples are NASA's Surface Biology and Geology (SBG) mission and the Copernicus Hyperspectral Imaging Mission for the Environment (CHIME), which is currently being developed by the European Commission and ESA. The overarching objective of the SBG, CHIME and the recently deployed PACE missions is to facilitate the acquisition of imaging spectroscopy data on a global coverage, with regular frequency and high spatial resolution.

In support to the Calibration and Validation activities of the hyperspectral PRISMA mission, Giardino et al. (2020) have reported that the PRISMA Top-Of-Atmosphere radiance ( $L_{TOA}$ ) of L1 products is consistent with the expected values over water targets; Braga et al. (2022) provided an initial evaluation of standard PRISMA L2 Rrs products (as distributed by ASI) and ACOLITE-derived Rrs over an inland and a coastal site; Pellegrino et al. (2023) evaluated the accuracy of PRISMA L2 products in visible and near-infrared spectral regions over 20 inland and coastal water sites worldwide.

One of the objectives of NECCTON is to provide CMEMS with new capability in fusing numerical model simulations and new and consolidated types of observations, including new hyperspectral observations from the PRISMA satellite mission. Multiple biogeochemical models will be upgraded by adding bio-optical modules describing the distribution of in-water irradiance along the water column and the interaction of optically active substances with the spectral light field. The integration of hyperspectral imagery and biogeochemical models by means of augmented skill-performance metrics and novel assimilation techniques is a challenging application for improving model parameters and enhancing the description of plankton and optically active properties. A prerequisite

<b>Project</b>	NECCTON No 101081273	<b>Deliverable</b>	4.2
<b>Dissemination</b>	Public	<b>Nature</b>	Report
<b>Date</b>	31 <sup>st</sup> December 2024	<b>Version</b>	1.0

for model validation and a successful data assimilation is an accurate estimation of uncertainties in the satellite observations. To this end, we explored the potential and limitations of PRISMA hyperspectral mission to provide reliable L2 products in coastal and marine sites, where PRISMA data are still underexploited. We present here the assessment of Rrs derived from PRISMA hyperspectral mission in aquatic sites, selected for biogeochemical model validation and data assimilation, using above-water *in situ* radiometry from autonomous hyper- and multispectral radiometer systems.

## 4. Study sites

The six study sites are listed in Table 1; their location is shown in Figure 1. Their characteristics are described in the following paragraphs.

Table 1. Sites included in the NECCTON Project.

Sites	Location	Geographic coordinates
Acqua Alta Oceanographic Tower (AAOT)	Northern Adriatic Sea	Lat. 45.314° N, Lon. 12.508° E
Casablanca Platform	Western Mediterranean Sea	Lat. 40.717° N, Lon. 1.358° E
Galata Platform	Western Black Sea	Lat. 43.045° N, Lon. 28.193° E
Section-7 Platform	Western Black Sea	Lat. 43.045° N, Lon. 28.193° E
Boussole Buoy	Ligurian Sea	Lat. 43.367° N, Lon. 7.900° E
L4 Scientific Buoy	Western English Channel	Lat. 50.250° N, Lon. 4.217° W

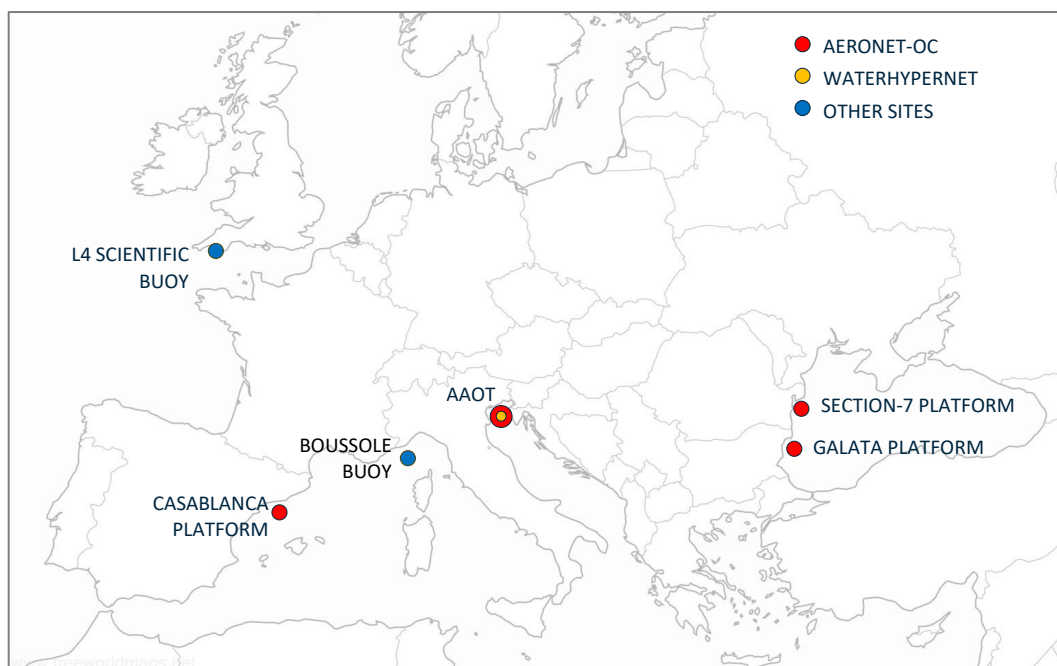


Figure 1. Map showing the NECCTON sites used for assessing PRISMA L2 imagery. Red dots identify AERONET-OC sites, whose radiometric data were used in this study. The yellow dot identifies the WATERHYPERNET site. Blue dots identify other sites.



<b>Project</b>	NECCON No 101081273	<b>Deliverable</b>	4.2
<b>Dissemination</b>	Public	<b>Nature</b>	Report
<b>Date</b>	31 <sup>st</sup> December 2024	<b>Version</b>	1.0

#### 4.1 Acqua Alta Oceanographic Tower

The Acqua Alta Oceanographic Tower (AAOT), located 15 km off the Venice lagoon in the northern Adriatic Sea, is both an AERONET-OC and a WATERHYPERNET network site, as described in the next chapter. AAOT is the longest operating AERONET-OC site with a series of measurements exceeding 20 years. The site is in a transitional region between open sea and coastal waters, and it is characterised by both Case-1 and Case-2 waters, with an occurrence of roughly 35% Case-2 waters moderately dominated by sediments. The aerosol type is mostly continental due to atmospheric inputs from the nearby Padana Plain (Zibordi et al., 2006; 2009a). Rrs values cover a fairly large dynamic range, with short-term variability (mostly dictated by regional river inputs) superimposed on an annual cycle showing larger values in winter-spring. Rrs maxima is usually observed in the spectral interval 490-560 nm.

#### 4.2 Casablanca Platform

This platform is situated in the Western Mediterranean Sea, about 40 km from the coast; it is the farthest site from the coast. Since April 2019, Casablanca Platform belongs to the AERONET-OC network. The site exhibits low turbidity and often Case-1 water conditions (i.e., with optical properties defined by phytoplankton and derivatives), with Rrs generally decreasing from the blue to low values in the red. Waters are characterised by low concentration of Chl $a$ , thus conducive to oligotrophic/mesotrophic Case 1 conditions (Zibordi et al., 2022; Cazzaniga and Melin, 2024).

#### 4.3 Galata Platform and Section-7 Platform

The Section-7 and Galata Platforms are both AERONET-OC sites located in the Western Black Sea. The first is positioned approximately 12 nautical miles from Romania, south of the Danube River mouth. The second platform is situated in a more southerly position, approximately 13 nautical miles offshore Bulgaria. Waters in this part of the Black Sea are optically complex, with Rrs maxima typically seen in the interval 490-560 nm (Cazzaniga and Zibordi, 2023). Section-7 can intermittently be influenced by the Danube River (Zibordi et al., 2022) and also undergoes the influence of coccolithophore blooms typically observed in summer (Cazzaniga et al., 2021; Kubryakov et al., 2021). These blooms can be responsible for large increases in the magnitude of Rrs (Berthon and Zibordi, 2008). Galata is situated further south on the shelf and does not feel the direct influence of the Danube.

#### 4.4 Boussole Buoy

The “BOUée pour l'acquiSition d'une Série Optique à Long termE” (BOUSSOLE) is situated in the Ligurian Sea, about 32 nautical miles (60 km) offshore the French Riviera and 60 nautical miles (110 km) from Corsica Island, into an area dedicated to moored scientific instruments on nautical charts. The water depth is 2440 m at the mooring point. The site has been hosting the BOUSSOLE bio-optical mooring since September 2003. It acquired multispectral radiometric measurements continuously at

<b>Project</b>	NECCTON No 101081273	<b>Deliverable</b>	4.2
<b>Dissemination</b>	Public	<b>Nature</b>	Report
<b>Date</b>	31 <sup>st</sup> December 2024	<b>Version</b>	1.0

high frequency (every 15 min) at two fixed depths (4 and 9 m). The site is mainly oligotrophic (chlorophyll-a concentration ranging between 0.05 and 5.0 mg m<sup>-3</sup>) with Case-1 water conditions (Antoine et al., 2006; 2008).

#### 4.5 L4 Scientific Buoy

L4 is a fixed station of the Western Channel Observatory, located in the Western English Channel on the North West European Shelf. It is situated 11 miles off the coast of Plymouth, 6.5 km away from the nearest land and significant riverine inputs. Water depth is roughly 50 m. L4 site is characterized by a dynamic water flow with semi-diurnal tide and riverine influences. Waters are seasonally stratified. It is a dynamic site with both terrestrial and oceanic influences, in a region of frontal activity. L4 is found to be classed as turbid for ~ 35% of the year (in winter) related to the vertical stability and suspended particulate matter. L4 can be considered as case 1 or case 2 depending upon the time period, the optical parameter or even the wavelength (Groom et al., 2009; Smyth et al., 2010).

## 5. Data

### 5.1 *In situ* radiometric data

One of the aims of the Task 4.4.1 of NECCTON Project was to determine the most suitable AC processing procedure for PRISMA images acquired over coastal and open sea aquatic areas. To accomplish this task, *in situ* radiometric data concomitant to PRISMA overpasses were gathered from fixed autonomous instruments for the assessment of PRISMA L2 dataset.

Four sites (AAOT, Casablanca Platform, Galata and Section-7 Platforms) belong to the AERONET-OC international network; AAOT is also included in the WATERHYPERNET network. Both are described in the following paragraphs. Standard PRISMA L2C images and PRISMA L1 images processed with other AC algorithms have been compared with the *in situ* radiometric measurements at these four sites.

#### 5.1.1 AERONET-OC network

The AErosol RObotic NETwork (AERONET) program (<https://aeronet.gsfc.nasa.gov>) is a federation of ground-based remote sensing aerosol monitoring network, developed to collect autonomous measurements of aerosol optical properties with sun photometers (Holben et al. 1998), that sustains atmospheric studies at various scales. The AERONET-Ocean Color (AERONET-OC) is a component of the program, developed specifically for supporting marine applications (see [https://aeronet.gsfc.nasa.gov/new\\_web/ocean\\_color.html](https://aeronet.gsfc.nasa.gov/new_web/ocean_color.html) for data access and site location) devoted to the validation of satellite ocean-color radiometry (Zibordi et al., 2006; 2010; Valente et al., 2019). AERONET-OC provides globally distributed standardized measurements of the water-leaving radiance accompanied by aerosol optical properties, with data available to the community in

<b>Project</b>	NECCON No 101081273	<b>Deliverable</b>	4.2
<b>Dissemination</b>	Public	<b>Nature</b>	Report
<b>Date</b>	31 <sup>st</sup> December 2024	<b>Version</b>	1.0

near-real time. The AERONET-OC sites are generally located offshore on lighthouses, oceanographic towers and oil platforms. They are equipped with an autonomous measurement system, the Sea-Viewing Wide Field-of-View Sensor (SeaWiFS) Photometer Revision for Incident Surface Measurements (SeaPRISM). The most recent SeaPRISM system configuration performs ocean color measurements in 11 spectral bands with a 10 nm bandwidth (400, 412.5, 442.5, 490, 510, 560, 620, 665, 779, 865 and 1020 nm) and with a full-angle field of view of 1.2° (Zibordi et al., 2009b). Bands at 865 and 1020 nm are used for quality checks. The acquisition geometry is described in detail in the AERONET-OC site ([https://aeronet.gsfc.nasa.gov/new\\_web/ocean\\_levels\\_versions.html](https://aeronet.gsfc.nasa.gov/new_web/ocean_levels_versions.html)). The measurement sequences are executed every 30 minutes within a time interval of  $\pm 4$  hours of 12:00 local time. The sequences include measurements of the direct sun irradiance for the retrieval of the atmospheric optical thickness, as this quantity is required to determine the water leaving radiance. Each sequence includes also a sequential set of sea radiance measurements, to determine the total radiance from the sea, and of sky radiance, both serially repeated for each band. If the sun is cloud covered, measurements are automatically stopped because of the low irradiance, and the whole measurement sequence is cancelled. The sequences are processed, and the results are made available in few hours from the acquisition.

In all AERONET-OC sites the same measuring systems and protocols are adopted (Sciuto et al., 2024), as well as the same processing procedures. All the instruments are calibrated using a single source and reference method and processed with the same code. Considering the characteristics of the NECCON sites, the normalized water-leaving radiance ( $L_{wn}$ ) corrected for bidirectional effects relying on the method proposed by Morel et al. (2002), identified as  $L_{wn\_f}/Q$ , has been used to obtain the *in situ* Rrs.  $L_{wn}$  were converted to Rrs by dividing by the mean extraterrestrial solar irradiance ( $F_0$ ) (Thuillier et al., 2003). AERONET-OC  $L_{wn}$  spectra are delivered at incremental levels of accuracy identified as Level 1.0, Level 1.5, and Level 2.0, according to the quality check procedures. The uncertainty in the determination of the normalized water-leaving radiance derived from SeaPRISM data is discussed in Zibordi et al. (2009b).

AERONET-OC data have been used to produce match-ups with satellite ocean colour data acquired within  $\pm 1$  hour from their acquisition. A sensitivity analysis on match-up as a function of time and spatial variability utilizing AERONET-OC data and different EO systems is presented in Zibordi et al., 2009a.

The main application of the AERONET-OC data is the validation of the Copernicus satellite data products, mostly from the Ocean & Land Colour Instruments (OLCI) on board Sentinel-3 (Donlon et al., 2012). The role of AERONET-OC is also important for the assessment of aquatic products associated with Sentinel-2 and Landsat 8 (Pahlevan et al., 2021) or with third-party missions, as PRISMA (Pellegrino et al., 2023).

### 5.1.2 WATERHYPERNET network

WATERHYPERNET is a prototype network of automated *in situ* measurements of hyperspectral water reflectance, recently established to provide data for satellite validation and water quality monitoring (Ruddick et al., 2024a). The network sites are equipped with two hyperspectral measurement

<b>Project</b>	NECCON No 101081273	<b>Deliverable</b>	4.2
<b>Dissemination</b>	Public	<b>Nature</b>	Report
<b>Date</b>	31 <sup>st</sup> December 2024	<b>Version</b>	1.0

systems: the Pan-and-Tilt Hyperspectral Radiometer (PANTHYR) and the HYperspectral Pointable System for Terrestrial and Aquatic Radiometry (HYPSTAR).

PANTHYR consists of two TriOS RAMSES radiometers (<https://www.trios.de/en/ramses.html>): one measures irradiance, the other measures radiance with a 7° Field of View. They operate in the 400-900nm range at 10nm Full Width Half Maximum (FWHM) with external camera mounted on a FLIR PTU-D48 E pan-tilt unit (Vansteenwegen et al., 2019).

HYPSTAR (<https://hypstar.eu/>) is a newly designed hyperspectral radiometer (Kuusk et al., 2024). It operates in the 380 – 1020nm range at 3nm FWHM. It integrates both radiance and irradiance fore-optics and is mounted on a Will-Burt Bowler Rx pan-tilt unit. It also has an embedded RGB camera. Both systems include auxiliary sensors for ambient light and rain detection. They are programmed to acquire data automatically every 20 minutes during daylight. Data acquisition follows a protocol based on Mobley (1999). After the acquisition, data are transmitted to a land station where an automatic quality check and processing procedure takes place.

WATERHYPERNET adopts the same approach as AERONET-OC for measurement of water-leaving radiance ( $L_w$ ), but makes direct measurement of downwelling irradiance ( $E_d$ ), using a flat diffuse collector with approximately cosine angular response instead of a sun photometer (see Ruddick et al., 2024a).

Recent applications of the WATERHYPERNET data are the validation of OLCI, Sentinel-2 and Landsat 8 (Dogliotti et al., 2024; Doxaran et al., 2024; Gonzalez Vilas et al., 2024). WATERHYPERNET is also important for the assessment of aquatic products associated with PRISMA (Braga et al., 2022; Dogliotti et al., 2024) and EnMAP (Soppa et al., 2024). According to Ruddick et al. (2024b), WATERHYPERNET is a prototype and some features still need to be implemented (i.e. complete uncertainty estimation, development of BRDF correction tools). However, data from WATERHYPERNET can already be intercompared directly with surface reflectance from AERONET-OC (Ruddick et al. 2024a). A more detailed comparison between both WATERHYPERNET and AERONET-OC instruments located at the same platform is expected to be performed in future to verify the consistency of the measurements (Gonzalez Vilas et al., 2024).

In this work, WATERHYPERNET data was used for the qualitative analysis only, given the limited number of match-ups available.

## 5.2 PRISMA hyperspectral imagery

PRISMA (*PR*ecursore *I*perSpettrale della *M*issione *A*pplicativa) is a scientific and demonstrative mission entirely financed by the ASI. It was launched on 22<sup>nd</sup> March 2019 and the operational life of the mission was planned to last five years. PRISMA, as a precursory mission, represents an advancement in Earth Observation technology, opening new opportunities to advance hyperspectral remote sensing methods, techniques and scientific data exploitation for innovative applications (Cogliati et al., 2021).

<b>Project</b>	NECCON No 101081273	<b>Deliverable</b>	4.2
<b>Dissemination</b>	Public	<b>Nature</b>	Report
<b>Date</b>	31 <sup>st</sup> December 2024	<b>Version</b>	1.0

PRISMA is a pushbroom imaging spectrometer based on prism technology and covers the nominal 400–2500 nm spectral range with two separated instruments:

- the Visible to Near-InfraRed (VNIR) spectrometer, which features 66 spectral bands from about 400 nm to 1010 nm, with a nominal spectral sampling interval lower than 11 nm and a bandwidth lower than 15 nm; the Short-Wave InfraRed (SWIR) detector, which provides 174 spectral bands between 920 and 2500 nm with a bandwidth lower than 15 nm.
- The panchromatic camera, which offers co-registered 5 m spatial resolution imagery useful for a better interpretation of the imaging spectrometer data.

PRISMA is flying on a Sun-Synchronous Low Earth Orbit at an altitude of 615 km. The nominal orbit re-visit time is 29 days (from nadir) with a re-look capability for a specific target of 7 days with off-nadir viewing. The nominal geographic coverage is between 70°S - 70°N latitude (at equinoxes) and 180°W - 180°E longitude, but imagery can be acquired at higher latitudes with the only limitation related to typically low solar zenith angle (SZA). The standard size of a single image is 30 × 30 km with a Ground Sampling Distance (GSD) of 30 m (VNIR-SWIR) and 5 m (PAN).

A comprehensive description of the PRISMA optical design and technical specifications for the hyperspectral imager and PAN instruments is available in (Coppo et al., 2020) and summarized in Table 2.

Table 2. PRISMA technical specifications: mission performance characterized by Leonardo Space & Airborne Systems. Modified from Cogliati et al., (2021).

	<b>VNIR</b>	<b>SWIR</b>	<b>PAN</b>
<b>Swath</b>	30 km	30 km	30 km
<b>Ground Sampling Distance (GSD)</b>	30 m	30 m	5 m
<b>Spectral Range</b>	400–1010 nm	920–2500 nm	400–700 nm
<b>Number of bands</b>	66	174	1
<b>Spectral Sampling Interval (SSI)</b>	7.2–11 nm	6.5–11 nm	–
<b>Spectral Resolution</b>	9–13 nm	9–14.5 nm	–
<b>Signal-to-Noise Ratio (SNR)</b>	161–209 (400–450 nm)	300–800 (1000–1300 nm)	191
	200–450 (450–1000 nm)	200–400 (1500–1750 nm)	–
	–	100–200 (1950–2350 nm)	–
<b>Absolute Radiometric Accuracy</b>	≤5% (Stability≤±1%)	≤5% (Stability≤±1%)	–

### 5.2.1 Standard PRISMA products

PRISMA data are systematically processed to provide standard products in three progressive levels (ASI, 2020):

<b>Project</b>	NECCTON No 101081273	<b>Deliverable</b>	4.2
<b>Dissemination</b>	Public	<b>Nature</b>	Report
<b>Date</b>	31 <sup>st</sup> December 2024	<b>Version</b>	1.0

- Level 0 (L0): formatted data products,
- Level 1 (L1): Top-Of-Atmosphere (TOA) radiance ( $L_{TOA}$ ) data radiometrically corrected and calibrated in physical units,
- Level 2 (L2): Bottom-Of-Atmosphere (BOA) atmospherically corrected images, obtained processing spectral  $L_{TOA}$  measurements. Level 2 products are available in three different sublevels:
  - L2B: geolocated ground spectral radiance products,
  - L2C: geolocated at-surface reflectance product, including aerosol characterization, water vapor, cloud characterization, observation and illumination geometry,
  - L2D: the geocoded version of L2C products.

L1 processor converts Level 0 raw imagery to  $L_{TOA}$  using a look-up table (LUT) transfer function from digital numbers to physical radiance units ( $mW\ m^{-2}sr^{-1}nm^{-1}$ ). L2 processor converts L1  $L_{TOA}$  to BOA Radiance or Reflectance. Details can be found in the PRISMA Algorithm Theoretical Basis Document (ASI, 2021).

## 5.2.2 PRISMA dataset for the present study

Access to mission capabilities and data is available through the ASI portal (<https://prisma.asi.it/>), after the user registration. The registration procedure requires the main user to declare the purposes of use of the original PRISMA products and to fill in the Project Form, including the personal data of any possible Contractor and/or Consultant and/or Affiliated User. Following the registration procedures, a specific account for NECCTON Project was assigned and login credentials were provided.

A total of 79 cloud-free PRISMA images in the VNIR spectral range, acquired from July 2019 to March 2024, were selected over the NECCTON sites (Table 3). L1 and L2C products were downloaded from the mission website and converted from original HDF-EOS5 (Hierarchical Data Format - Earth Observing System) file to band sequential file format using ENVI 5.7 (L3Harris Technologies, USA). Since strong improvements of the mission ground processor and the data product quality were achieved from the launch, we used L1 and L2C data processed by the last standard PRISMA mission ground processor version L1-4.1.0 and AC processor version L2-02.05, respectively.

Table 3. Spatial and temporal coverages of PRISMA images at the six NECCTON sites.

Test site	n. of PRISMA images	Temporal coverage
Acqua Alta Oceanographic Tower	16	July 2019 – March 2023
Casablanca Platform	13	April 2021 – March 2024
Galata Platform	24	April 2020 – October 2023
Section-7 Platform	18	July 2021 – September 2023
Boussole Buoy	4	August 2022 – June 2023
L4 Scientific Buoy	4	June 2021 – October 2022

<b>Project</b>	NECCON No 101081273	<b>Deliverable</b>	4.2
<b>Dissemination</b>	Public	<b>Nature</b>	Report
<b>Date</b>	31 <sup>st</sup> December 2024	<b>Version</b>	1.0

## 6. Methodology

### 6.1 Atmospheric correction processors

#### 6.1.1 Standard L2C processor

The Standard L2C processor converts TOA spectral radiance measurement L1 into geophysical parameters providing the geolocated BOA signal L2C in reflectance units. It includes two procedures: the atmospheric correction and geometric correction. Besides the at-surface reflectance, Level-2C products provide additional maps related to atmospheric constituents, computed starting from the observed scene: water vapor columnar, content, aerosol optical thickness, angstrom exponent, cloud optical thickness.

The Standard L2C processor is based on MODTRAN 6.0, using a multi-dimensional look-up table (LUT) approach (ASI, 2021) with the following auxiliary data:

- Solar irradiance,
- LUTs containing simulated geophysical observations obtained through a radiative transfer code,
- A digital elevation model.

The LUT entails simulated  $L_{TOA}$ , obtained through a radiative transfer model.  $L_{TOA}$  is pre-computed, stored and indexed as a function of geometric condition (sun zenith angle, relative azimuth angle and view zenith angle) and different atmospheric scenario based on atmospheric model (mid-latitude winter and summer), ground altitude, water vapour, and aerosol optical thickness. Results from simulations are stored in LUTs and the AC processor reads the LUTs pertaining to each parameter space and interpolates if required. The aerosol model used to build LUTs is limited to the rural model provided by MODTRAN6 library. According to the PRISMA Products Specification Document (ASI, 2020), to remove the effects of the atmosphere, first the Water Vapor columnar content (WV) for each pixel is retrieved using the water band at  $1.13\mu\text{m}$ . The Aerosol Optical Depth (AOT) is then estimated for the whole scene. The retrieval of AOT is based on the Dense Dark Vegetation (DDV) algorithm approach, exploiting the correlation between reflectance in the SWIR region and the blue and red bands. If the scene contains no dark pixels suitable for the retrieval of AOT, the AC processor uses a default constant value. The inverse radiative transfer equation for the given AOT and WV is solved by using an iterative method. This procedure calculates the radiance emerging from the Earth surface (Level 2B) and the ratio between the emerging and the incoming radiance at the surface (Level 2C). Surface reflectance Level 2C products are directly used for application purposes since they already contain geophysical and geo-coded information. PRISMA surface reflectance Level 2C products were converted to remote sensing reflectance by dividing by  $\pi$  and were used for the match-up analysis; for sake of clarity, these products will still be referred to as L2C, despite the use of  $\pi$ .



<b>Project</b>	NECCON No 101081273	<b>Deliverable</b>	4.2
<b>Dissemination</b>	Public	<b>Nature</b>	Report
<b>Date</b>	31 <sup>st</sup> December 2024	<b>Version</b>	1.0

The AC processor has been designed for land applications; in particular, the aerosol rural model from the MODTRAN library is not optimal for the analysis of images acquired on aquatic environments (Braga et al., 2022).

### 6.1.2 ACOLITE

ACOLITE, developed at Royal Belgian Institute of Natural Sciences, is a software developed for the AC of satellite images for aquatic applications. It is applicable to images acquired by numerous satellite sensors, among which Landsat 8/9 (Vanhellemont and Ruddick, 2014), Sentinel-2 MSI (Vanhellemont and Ruddick, 2016; Vanhellemont, 2019; 2020) and Sentinel-3 OLCI (Vanhellemont and Ruddick, 2021), and to data acquired by several hyperspectral missions, including PRISMA (Braga et al., 2022) and EnMAP (Soppa et al., 2024). ACOLITE is available on GitHub (<https://github.com/acolite/acolite>); in this study, the version 20231023.0 has been used, without and with the option of glint correction.

ACOLITE is based on the Dark Spectrum Fitting (DSF) approach (Vanhellemont, 2019; 2020) in which multiple dark targets in the scene or subscene are chosen to construct a dark spectrum. This is then used to estimate the AOT at 550 and atmospheric path reflectance according to the best-fitting aerosol model. The AOT and aerosol type were imposed to be fixed over the 30 × 30 km PRISMA acquisition. ACOLITE used the Continental and Maritime aerosol models from 6SV.

For ACOLITE DSF processing both a PRISMA L1 image and the matching L2C data are required as inputs. At runtime, band specific Gaussian relative spectral response functions are generated for both VNIR and SWIR detectors, using the central wavelength and FWHM information provided in the HDF5 metadata. Geometry information is currently not included in the L1 data, and hence the per-pixel sun and view geometry (i.e. sun and view zenith and relative azimuth angles) is extracted from the matching L2C file. Rrs is output by dividing the corrected water reflectance by  $\pi$ . Hereafter we will refer to Rrs obtained from the ACOLITE atmospheric correction of PRISMA L1 as ACOLITE DSF.

In addition to the DSF procedure, ACOLITE has an optional image-based sun glint correction (Vanhellemont, 2019). This correction is performed by estimating the interface reflectance signal in the SWIR from the average  $\rho_s$  between 1500 and 2400 nm - i.e. assuming zero water leaving radiance in this spectral range. To extend this average SWIR observation towards the VNIR, the interface reflectance is modelled with OSOAA (Chami et al., 2015) for the current scene average sun-sensor geometry, the estimated aerosol model and AOT for a high ( $20 \text{ m s}^{-1}$ ) wind speed. Remote sensing reflectance is output by dividing the air–water interface reflectance corrected water reflectance by  $\pi$  and hereafter we will refer to it as ACOLITE DSF + GC.

Another setting of ACOLITE was applied using a user specified aerosol optical thickness (AOT) value at 550 nm for the Dark Spectrum Fitting. The AOT values were gathered from AERONET-OC data. Remote sensing reflectance is output by dividing the corrected water reflectance by  $\pi$ . Hereafter we will refer to Rrs obtained from the ACOLITE AC of PRISMA L1 with fixed AOT as ACOLITE AOT.



<b>Project</b>	NECCON No 101081273	<b>Deliverable</b>	4.2
<b>Dissemination</b>	Public	<b>Nature</b>	Report
<b>Date</b>	31 <sup>st</sup> December 2024	<b>Version</b>	1.0

### 6.1.3 POLYMER

The POLYMER software, developed by HYGEOS, is an AC algorithm purposely developed for retrieving the ocean colour when the observation is contaminated by the sun glint (Steinmetz et al., 2011; Steinmetz and Ramon, 2018). It has been developed for MERIS on Envisat and is currently applicable to images acquired by other sensors: MODIS Aqua, SeaWiFS, VIIRS, Sentinel-3 OLCI, Sentinel-2 MSI, PRISMA, HICO and EnMAP. POLYMER is available on GitHub (<https://github.com/hygeos/polymer>); in this study the version 4.17beta2 has been used.

The POLYMER algorithm uses the image bands in the whole spectral range from the blue to the near infrared, to decouple the atmospheric and surface components of the signal from the water reflectance. The bands near strong atmospheric absorption features are filtered out. The algorithm relies on two models, an analytical model for the atmosphere which uses a second-order polynomial formulation with respect to the wavelength, and a water reflectance model based on two parameters, one for the chlorophyll concentration and one for the backscattering coefficient. The latter is based on the bio-optical model of Park and Ruddick (2005). Water-leaving reflectance is further normalised to the nominal wavelength and for the water-leaving reflectance bidirectional effects (BRDF), such that the radiometric output of Polymer is the fully normalised water-leaving reflectance spectrum corrected for bidirectional effects.

Detailed information on the pre-correction (e.g., estimation of the gaseous transmittance, Rayleigh scattering, and pre-glint correction), spectral matching, and the atmospheric model was presented in Steinmetz et al. (2011) and Steinmetz and Ramon (2018); information on the water-leaving reflectance model can be found in Park and Ruddick (2005) and its modifications, water-leaving reflectance normalisation, and BRDF correction were described in Steinmetz and Ramon (2018).

Rrs is output by dividing the corrected normalised water-leaving reflectance by  $\pi$  and hereafter we will refer to it as POLYMER.

## 6.2 Match-up analysis

The satellite extract is usually defined as a box of a specified number of pixels centred on the location of the *in situ* measurement (Concha et al. 2021). In some cases, the centre of the extract is discarded or displaced to avoid contaminations at pixel or sub-pixel level due to the instrument platform (e.g. impact of platform and/or platform shadows within high spatial resolution pixels) (Ilori et al., 2019; Vanhellemont, 2019; Pahlevan et al., 2021; Braga et al., 2022).

In this study, the Region Of Interest (ROI) of PRISMA data was generated for each scene by (1) extracting a 8 x 8 pixel window centred on the location of the AERONET-OC site, and (2) removing the centre 6 x 6 pixels from that window to limit the perturbations from the site's structures and shadows. An example for Section-7 Platform is shown in Figure 2. Once generated, the ROIs have been used to extract values from the L2C PRISMA images and from the PRISMA images corrected with the AC processors.

<b>Project</b>	NECTON No 101081273	<b>Deliverable</b>	4.2
<b>Dissemination</b>	Public	<b>Nature</b>	Report
<b>Date</b>	31 <sup>st</sup> December 2024	<b>Version</b>	1.0

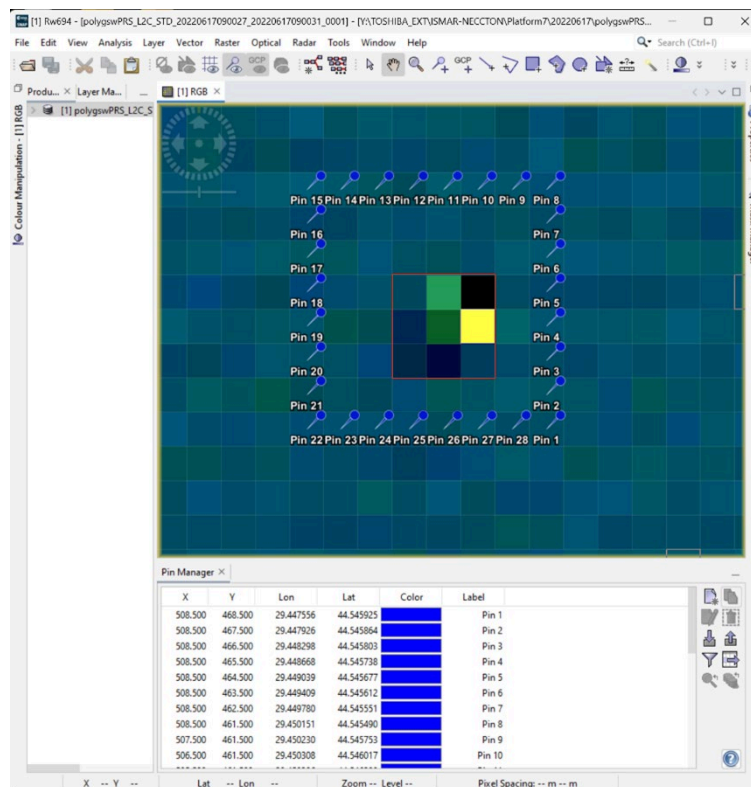


Figure 2. Example of the ROI built as a 8x8 frame around Section-7 Platform (28 pins). The background image is a true-color composite of the PRISMA image acquired on 17<sup>th</sup> June 2022, and corrected with POLYMER: red 665nm, green 575, blue 483nm. The platform area and the pixels contaminated from the platform's shadow are outlined in red. Software: Sentinel Application Platform – SNAP (ESA- European Space Agency).

The validation process compares data collected on different spatial scales (*in situ* point measurements versus satellite pixel-size data), that can be affected by heterogeneous conditions. To exclude satellite pixels affected by a high spatial variability within the ROI, a spatial homogeneity check was performed, similarly to Bailey and Werdell (2006). The filtered mean value of the extract was used for the match-up, i.e. considering only the pixel values that fell between the median  $\pm 1.5^*$  standard deviation, evaluated on the pixels box. A time window of  $\pm 1$  h between *in situ* and satellite data was considered for the match-up analysis to reduce uncertainties related to temporal variability (e.g. coastal waters with tidal effects or affected by river discharge), according to Zibordi et al. (2009a) and Vanhellemont and Ruddick (2021). Finally, as the spectral band-set of AERONET-OC and PRISMA data differs for band centre and FWHM, prior to the comparison, spectral sampling and binning procedures are applied to the PRISMA data to obtain the same bandcenter and bandwidth of AERONET-OC data.

At first, a qualitative comparison of mean PRISMA Rrs as derived from L2C, ACOLITE DSF, ACOLITE DSF+GC and POLYMER, at their original spectral resolutions, versus *in situ* radiometric data, was performed in the range of 400–900 nm. A quantitative analysis of *in situ* multispectral data and resampled PRISMA spectra was performed for each site. Then, a set of descriptive statistics has been

<b>Project</b>	NECCON No 101081273	<b>Deliverable</b>	4.2
<b>Dissemination</b>	Public	<b>Nature</b>	Report
<b>Date</b>	31 <sup>st</sup> December 2024	<b>Version</b>	1.0

calculated to assess the consistency between the reference dataset (AERONET-OC measurements) and the values obtained from the atmospheric-processed PRISMA images.

Validation is the process of comparing satellite products, i.e. the Rrs obtained through the atmospheric correction and the spectral resampling procedure, henceforth indicated in the formulas as  $(Rrs(\lambda)_{sat,i})_{i=1,n'}$  with reference data, i.e. the AERONET-OC field observations, henceforth indicated in the formulas as  $(Rrs(\lambda)_{insitu,i})_{i=1,n}$ . The descriptive statistics were selected among the ones proposed by the literature (Concha et al., 2021; Pahlevan et al., 2021; Warren et al., 2019): the Coefficient of Determination  $R^2$ , the Root Mean Square Difference (RMSD), the Mean Absolute Difference (MAD), the Mean Absolute Percent Difference (MAPD). In addition, the Spectral Angle (SA), proposed by Kruse et al. (1993), was calculated. The descriptive statistics are shown in Table 4.

Table 4. Statistical metrics used to assess the agreement of Rrs among the datasets; n is the number of concurrent observations of the match-up;  $Rrs(\lambda)_{sat,i}$  and  $Rrs(\lambda)_{insitu,i}$  are the  $i^{th}$  satellite-derived and *in situ* measurement for the variable Rrs for the band center  $\lambda$ , respectively.  $Rrs(d)_{sat}$  and  $Rrs(d)_{insitu}$  are the vectors of Rrs measurements over all wavelengths, respectively derived from PRISMA and from *in situ* AERONET-OC measurements, at date d.

<b>Coefficient of Determination <math>R^2</math></b>  In this context, measures how well the atmospherically corrected data fit a linear regression with the <i>in situ</i> data. Values near to 1 indicate best fit. In this case (a single dependent variable) it is equal to the squared value of the Pearson correlation coefficient.	$R^2 = \left[ \frac{\sum_{i=1}^n (Rrs(\lambda)_{insitu,i} - \overline{Rrs(\lambda)_{insitu}}) (Rrs(\lambda)_{sat,i} - \overline{Rrs(\lambda)_{sat}})}{\sqrt{\sum_{i=1}^n (Rrs(\lambda)_{insitu,i} - \overline{Rrs(\lambda)_{insitu}})^2} \sqrt{\sum_{i=1}^n (Rrs(\lambda)_{sat,i} - \overline{Rrs(\lambda)_{sat}})^2}} \right]^2$
<b>Root Mean Square Difference or Deviation (RMSD)</b>  Calculates the root mean square differences between <i>in situ</i> values and the values of the atmospherically corrected data. It allows to compare forecasting errors of different AC algorithms for an <i>in situ</i> dataset.	$RMSD(\lambda) = \sqrt{\frac{1}{N} \sum_{i=1}^N (Rrs(\lambda)_{sat,i} - Rrs(\lambda)_{insitu,i})^2}$
<b>Mean Absolute Difference (MAD)</b>  MAD is the average of the absolute values of the differences between the model (atmospherically corrected) data and the actual values ( <i>in situ</i> ) data. Low values indicate high processing accuracy.	$MAD(\lambda) = \frac{1}{N} \sum_{i=1}^N  Rrs(\lambda)_{sat,i} - Rrs(\lambda)_{insitu,i} $
<b>Mean Absolute Percent Difference (MAPD)</b>  Measures the percentage difference between the model (satellite data) and the actual values ( <i>in situ</i> data). Low percentages indicate high processing accuracy.	$MAPD(\lambda) = 100 \cdot \frac{1}{N} \left( \sum_{i=1}^N \frac{ Rrs(\lambda)_{sat,i} - Rrs(\lambda)_{insitu,i} }{Rrs(\lambda)_{insitu,i}} \right)$
<b>Spectral Angle (SA)</b>  Expresses the angle between image spectra and <i>in situ</i> spectra in the band space. Low values indicate great similarity.	$SA = \cos^{-1} \left( \frac{\sum_{i=1}^N Rrs(d)_{sat,i} \cdot Rrs(d)_{insitu,i}}{\sqrt{\sum_{i=1}^N Rrs(d)_{sat,i}^2} \cdot \sqrt{\sum_{i=1}^N Rrs(d)_{insitu,i}^2}} \right)$

<b>Project</b>	NECCTON No 101081273	<b>Deliverable</b>	4.2
<b>Dissemination</b>	Public	<b>Nature</b>	Report
<b>Date</b>	31 <sup>st</sup> December 2024	<b>Version</b>	1.0

## 7. Results

The match-up analysis was carried out on data collected from July 2019 to March 2024. A total of 79 PRISMA images was processed for six test sites, as shown in Table 3. Validation results for PRISMA Rrs are illustrated as qualitative and quantitative comparisons. The main purpose of the qualitative comparison is to showcase for each date the different match-ups included in the analysis, to highlight the wide variability of Rrs spectra and/or to point out artefacts that may characterise either satellite or *in situ* data. Quantitative comparison is shown with associated statistics for each site considering the AERONET-OC bands. The number of match-ups varies as a function of the acquisition of PRISMA and the availability of concomitant AERONET-OC measurements. For the objective of the NECCTON project, PRISMA images acquired over L4 and Boussole sites were also processed with the atmospheric correction processors, although no *in situ* data was available for validation. For these sites, only a qualitative comparison of PRISMA Rrs was performed.

### 7.1 Qualitative analysis

The qualitative comparison of the *in situ* Rrs, derived from the normalized water-leaving radiance from AERONET-OC, and the Rrs spectra from PRISMA, processed using the three AC processors, is shown at their original spectral resolutions in Figure 3 for AAOT, Figure 4 for Casablanca Platform, Figure 5 and Figure 6 for Galata Platform, Figure 7 for Section-7 Platform. Additional *in situ* hyperspectral measurements from WATERHYPERNET systems are also shown for AAOT (Figure 3). The qualitative comparison of PRISMA Rrs over L4 and Boussole sites are shown in Figure 8 and Figure 9, respectively.

As expected, the reflectance spectra differed greatly in magnitude and shape, due to very different characteristics of the sites and their large optical diversity. Casablanca Platform, characterized by oligotrophic waters, likely representing Case-1 condition, exhibits maxima at the blue center-wavelengths and negligible values above 600 nm. The same shape can be appreciated in the spectra obtained at Boussole, particularly in the data corrected with ACOLITE - plus glint correction - and POLYMER. At coastal sites with moderately turbid waters (AAOT, Section-7, Galata, L4), the local maximum around 500 nm and non-negligible values in the 650–700 nm range are typical of oligotrophic/mesotrophic water, slightly influenced by suspended particles. In some dates, Section-7 shows the local maxima at 560 nm, due to seasonal algal blooms or related to large increases in suspended and dissolved matter from Danube River (Zibordi et al., 2021). An example of both effects on water colour is shown in Figure 10 for the Section-7 Platform. A significant variability in magnitude and spectral shape was also visible at AAOT and Galata sites, caused by the wide range of bio-optical properties influenced by seasonal conditions and meteorological forcing (Cazzaniga and Melin, 2024). Overall, the Rrs spectra are representative of the variability observed in Zibordi et al. (2021).

A more detailed analysis of the spectral curves highlights that in general the L2C processor and the ACOLITE AOT products show the widest differences from the *in situ* AERONET-OC spectral data. The differences are higher in the shorter wavelengths, up to 560nm. These uncertainties could be due to

<b>Project</b>	NECCTON No 101081273	<b>Deliverable</b>	4.2
<b>Dissemination</b>	Public	<b>Nature</b>	Report
<b>Date</b>	31 <sup>st</sup> December 2024	<b>Version</b>	1.0

the inaccurate estimation of AOT or the aerosol model used in the AC procedure. Furthermore, lower SNR of PRISMA L1 at these wavelengths can even yield higher uncertainties (Braga et al., 2022). The deviation of L2C with respect to *in situ* data is remarkable on some dates, while Rrs derived from POLYMER matched quite well. This likely resulted from the values of AOT used in the AC inversion. In fact, the retrievals of aerosol properties in L2C processor (land-based) and in ACOLITE and POLYMER are based on different approaches (water-based).

Another issue that could affect the match-ups is the effect of sun-glint on Rrs, which is corrected in ACOLITE/DSF + GC spectra and POLYMER, but it can still impact ACOLITE/DSF and L2C data, as likely on 31<sup>st</sup> May 2022 at Galata (Figure 11) and on 9<sup>th</sup> August 2023 at Section-7. On these dates, L2C and ACOLITE spectra increased by a factor of 0.5 or more due to sun-glint, although they looked very similar in shape to the spectra with glint correction (Figure 6 and Figure 7). A more dramatic case of sun glint is present in the image acquired on 23<sup>rd</sup> June 2023 at Boussole; in this case, the entire image is affected (Figure 12). While the POLYMER spectrum appears unaffected (Figure 8), both the values of ACOLITE DSF and ACOLITE DSF plus glint correction are doubled, and the values of L2C are even greater. It is relevant to notice that the values for ACOLITE and ACOLITE DSF+GC are almost identical, and that they increase slightly with increasing wavelengths: the glint correction appears to have been influential on the output spectral shapes as well as on values.

Rrs is also affected by wind speed (sea state), that can influence the air-water interface reflectance, increasing the reflected skylight. For wind speeds higher than 12 m/s, the disturbance due to white-capping, foam, bubbles, and spray must be considered. An example is the PRISMA image of 11<sup>th</sup> March 2024 at Casablanca, where the wind speed was about 9 m/s (Figure 13).

The spectral curves also show the presence of negative values in the longer wavelengths range. They may occur in ACOLITE images at wavelengths greater than 800 nm and are common in POLYMER images at wavelengths greater than 700 nm. In contrast, negative values are never present in L2C images. This limits the present capability of POLYMER to the correction of PRISMA bands in the range up to 700 nm. Other important elements can be drawn from the observation of the spectral curves. A most noticeable one is the presence of anomalously high values or “spikes”. While *in situ* measured water spectra are rather smooth, the PRISMA data show band-to-band spectral variations, especially in the 400–560 nm region. These spectral spikes are likely the result of inter-band calibration issues (Lavigne et al., 2021). The spikes are present – albeit to different extents - in the spectral curves of all the corrected images at the following wavelengths: 431, 489, 512, 592, 723, 764 and 902 nm. It has therefore been decided to discard these wavelengths in the subsequent quantitative analysis, as well as the values measured at wavelengths beyond 902 nm.

<b>Project</b>	NECTON No 101081273	<b>Deliverable</b>	4.2
<b>Dissemination</b>	Public	<b>Nature</b>	Report
<b>Date</b>	31 <sup>st</sup> December 2024	<b>Version</b>	1.0

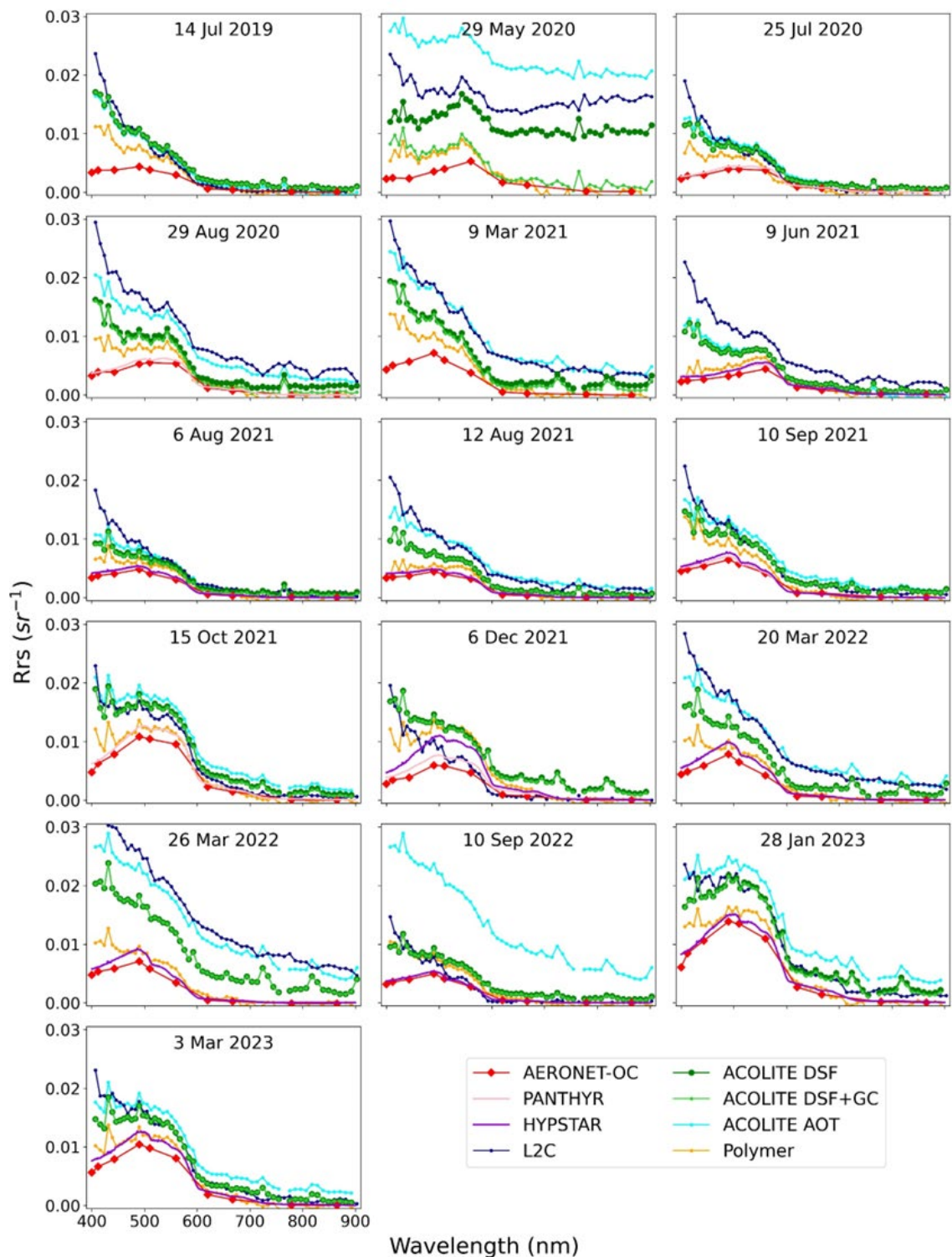


Figure 3. Qualitative comparison of  $R_{rs}$  at AAOT site. *In situ*  $R_{rs}$  obtained from autonomous radiometer systems: AERONET-OC (red), PANTHYR (pink) and HYPSTAR (purple). PRISMA  $R_{rs}$  processed using: L2C (blue); ACOLITE with the dark spectrum fitting algorithm (ACOLITE DSF) (green), with the addition of sun-glint correction (ACOLITE DSF + GC) (light green), with the fixed AOT value (ACOLITE AOT) (cyan); POLYMER (yellow).



<b>Project</b>	NECTON No 101081273	<b>Deliverable</b>	4.2
<b>Dissemination</b>	Public	<b>Nature</b>	Report
<b>Date</b>	31 <sup>st</sup> December 2024	<b>Version</b>	1.0

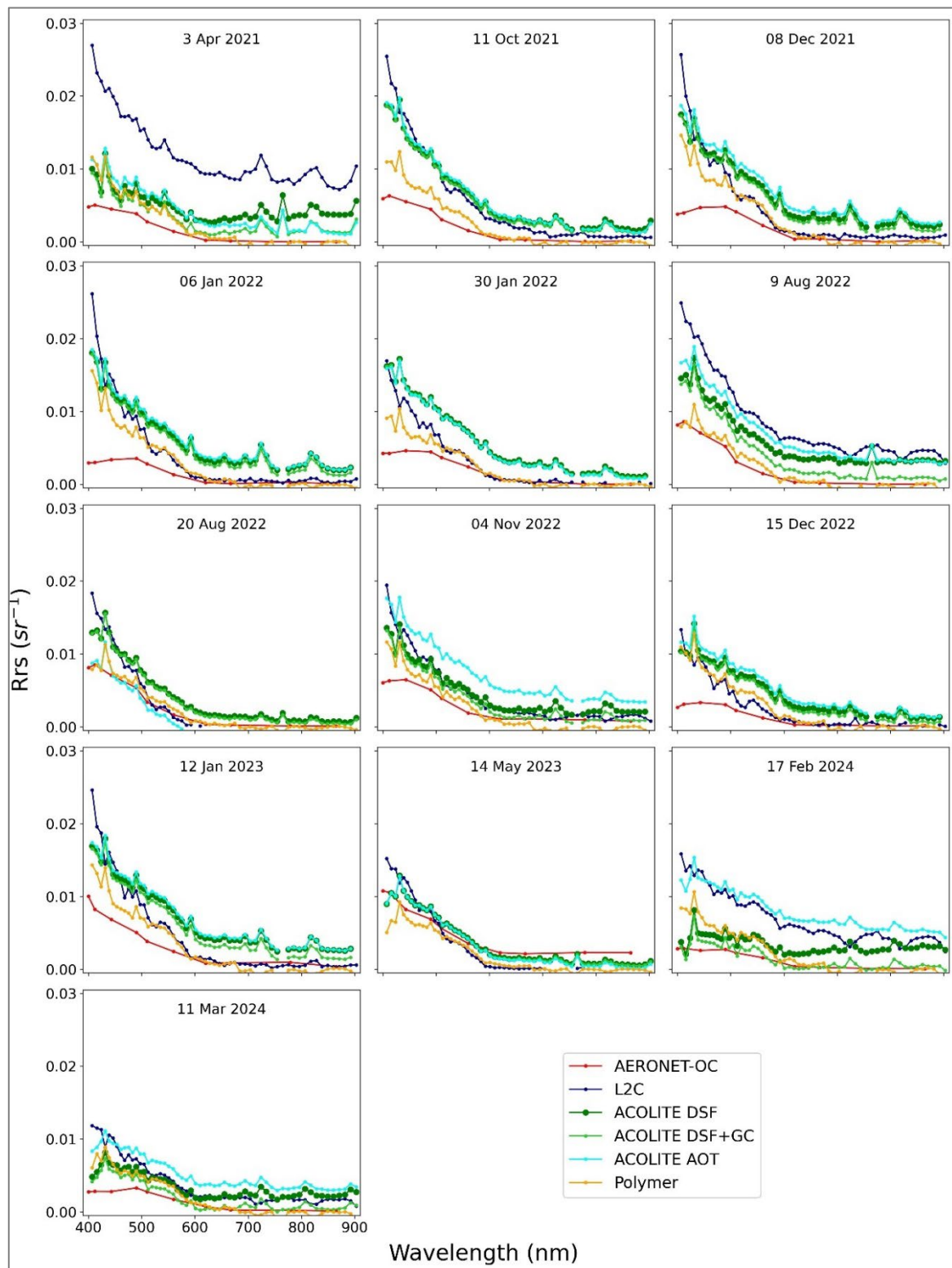


Figure 4. Qualitative comparison of Rrs at Casablanca Platform. *In situ* Rrs obtained from AERONET-OC (red). PRISMA Rrs processed using: L2C (blue); ACOLITE with the dark spectrum fitting algorithm (ACOLITE DSF) (green), with the addition of sun-glint correction (ACOLITE DSF + GC) (light green), with the fixed AOT value (ACOLITE AOT) (cyan); POLYMER (yellow).

<b>Project</b>	NECTON No 101081273	<b>Deliverable</b>	4.2
<b>Dissemination</b>	Public	<b>Nature</b>	Report
<b>Date</b>	31 <sup>st</sup> December 2024	<b>Version</b>	1.0

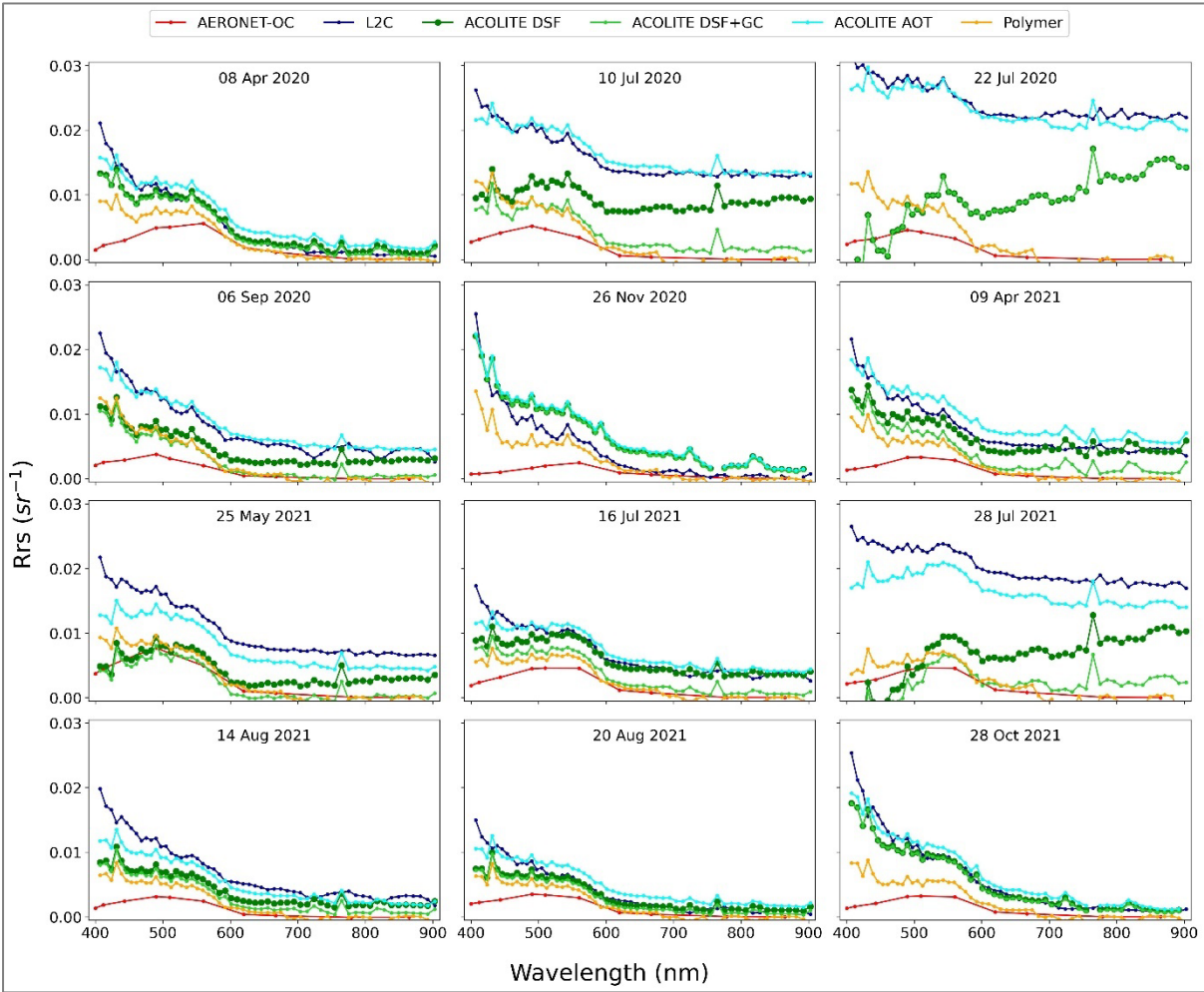


Figure 5. 1/2 Qualitative comparison of  $R_{rs}$  at Galata Platform (from 8<sup>th</sup> April 2020 to 28<sup>th</sup> October 2021). *In situ*  $R_{rs}$  obtained from AERONET-OC (red). PRISMA  $R_{rs}$  processed using: L2C (blue); ACOLITE with the dark spectrum fitting algorithm (ACOLITE DSF) (green), with the addition of sun-glint correction (ACOLITE DSF + GC) (light green), with the fixed AOT value (ACOLITE AOT) (cyan); POLYMER (yellow).



<b>Project</b>	NECTON No 101081273	<b>Deliverable</b>	4.2
<b>Dissemination</b>	Public	<b>Nature</b>	Report
<b>Date</b>	31 <sup>st</sup> December 2024	<b>Version</b>	1.0

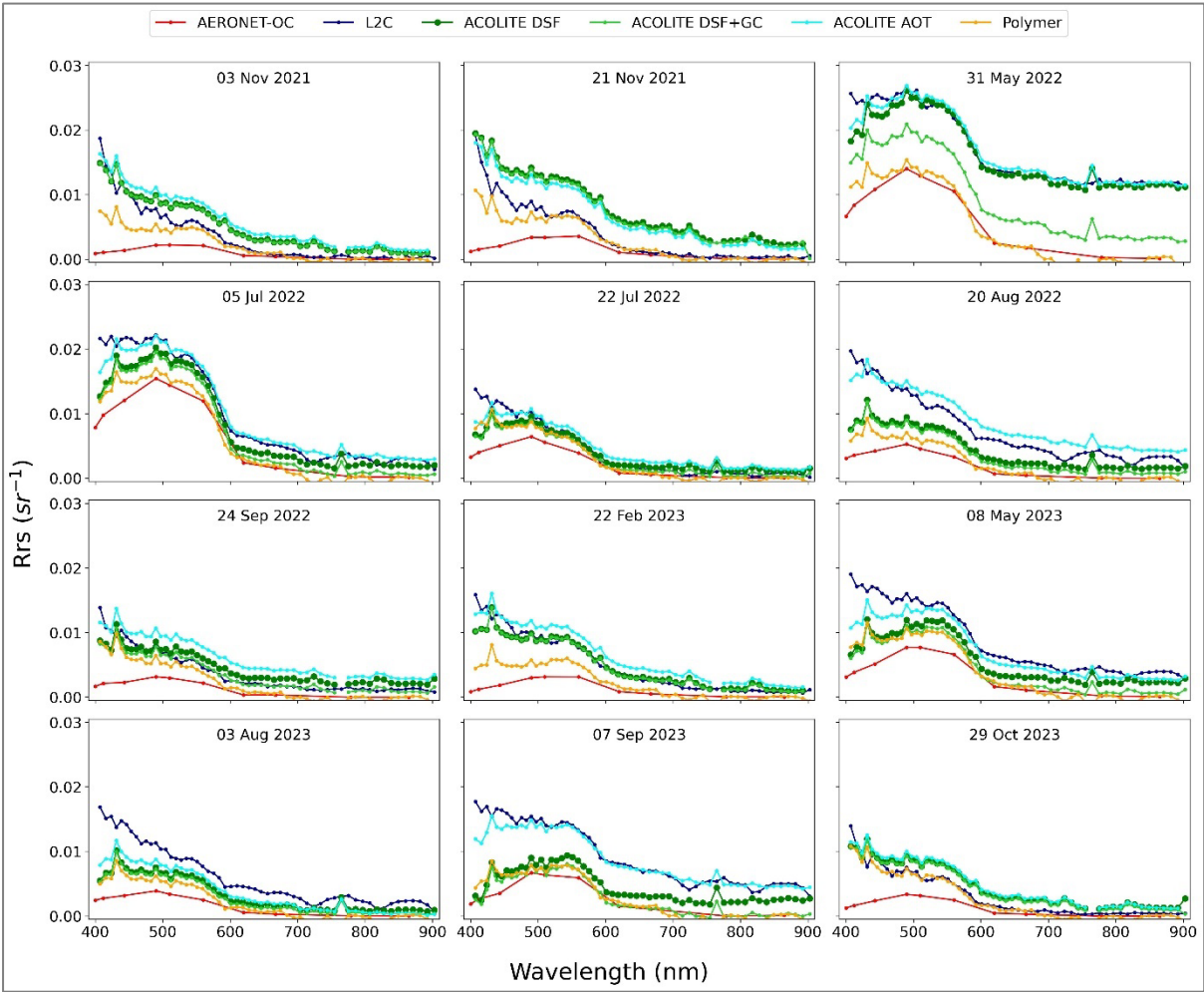


Figure 6. 2/2 Qualitative comparison of Rrs at Galata Platform (from 3<sup>rd</sup> November 2021 to 29<sup>th</sup> October 2023). *In situ* Rrs obtained from AERONET-OC (red). PRISMA Rrs processed using: L2C (blue); ACOLITE with the dark spectrum fitting algorithm (ACOLITE DSF) (green), with the addition of sun-glint correction (ACOLITE DSF + GC) (light green), with the fixed AOT value (ACOLITE AOT) (cyan); POLYMER (yellow).

<b>Project</b>	NECTON No 101081273	<b>Deliverable</b>	4.2
<b>Dissemination</b>	Public	<b>Nature</b>	Report
<b>Date</b>	31 <sup>st</sup> December 2024	<b>Version</b>	1.0

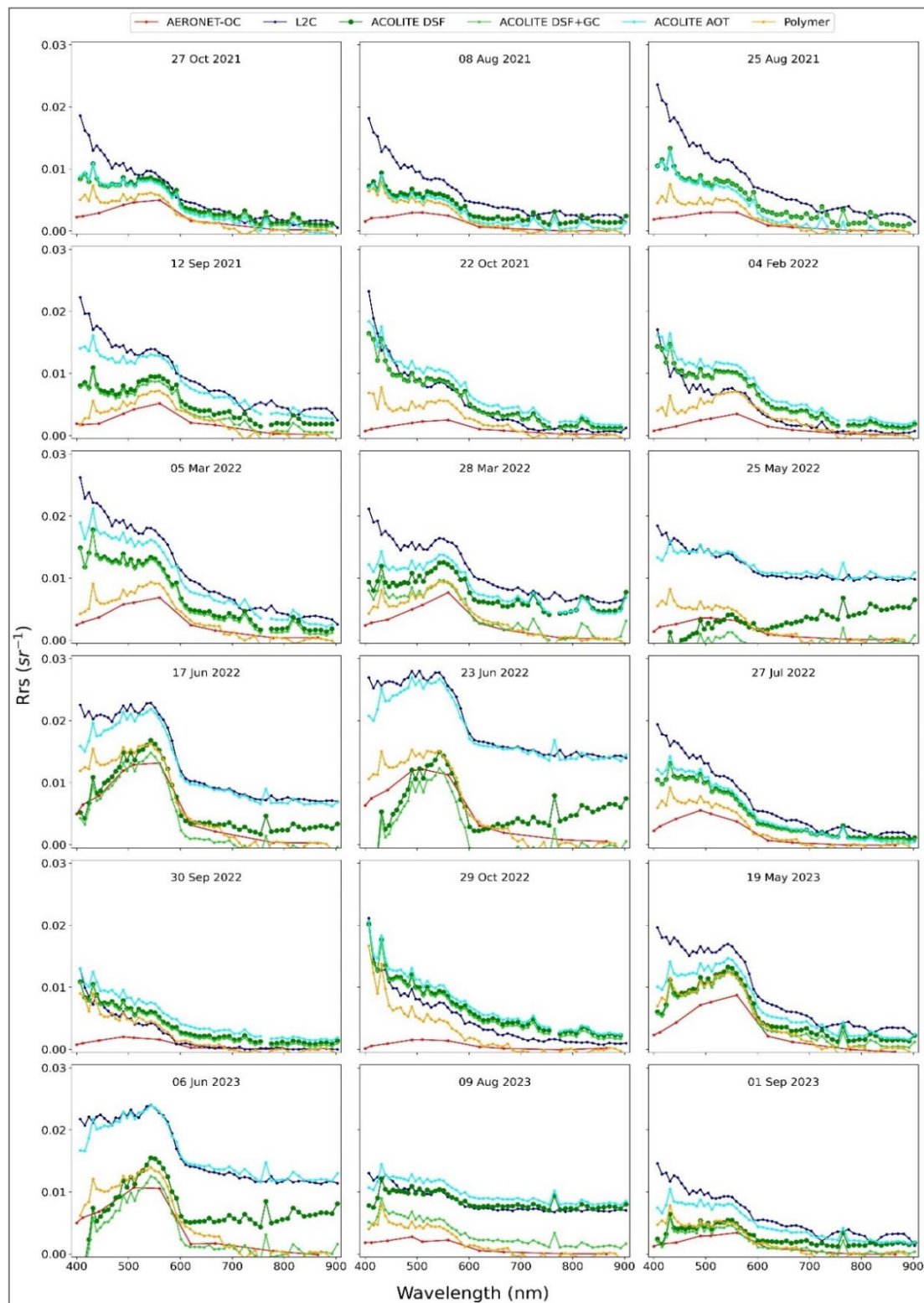


Figure 7. Qualitative comparison of Rrs at Section-7 Platform. *In situ* Rrs obtained from AERONET-OC (red). PRISMA Rrs processed using: L2C (blue); ACOLITE with the dark spectrum fitting algorithm (ACOLITE DSF) (green), with the addition of sun-glint correction (ACOLITE DSF + GC) (light green), with the fixed AOT value (ACOLITE AOT) (cyan); POLYMER (yellow).

<b>Project</b>	NECTON No 101081273	<b>Deliverable</b>	4.2
<b>Dissemination</b>	Public	<b>Nature</b>	Report
<b>Date</b>	31 <sup>st</sup> December 2024	<b>Version</b>	1.0

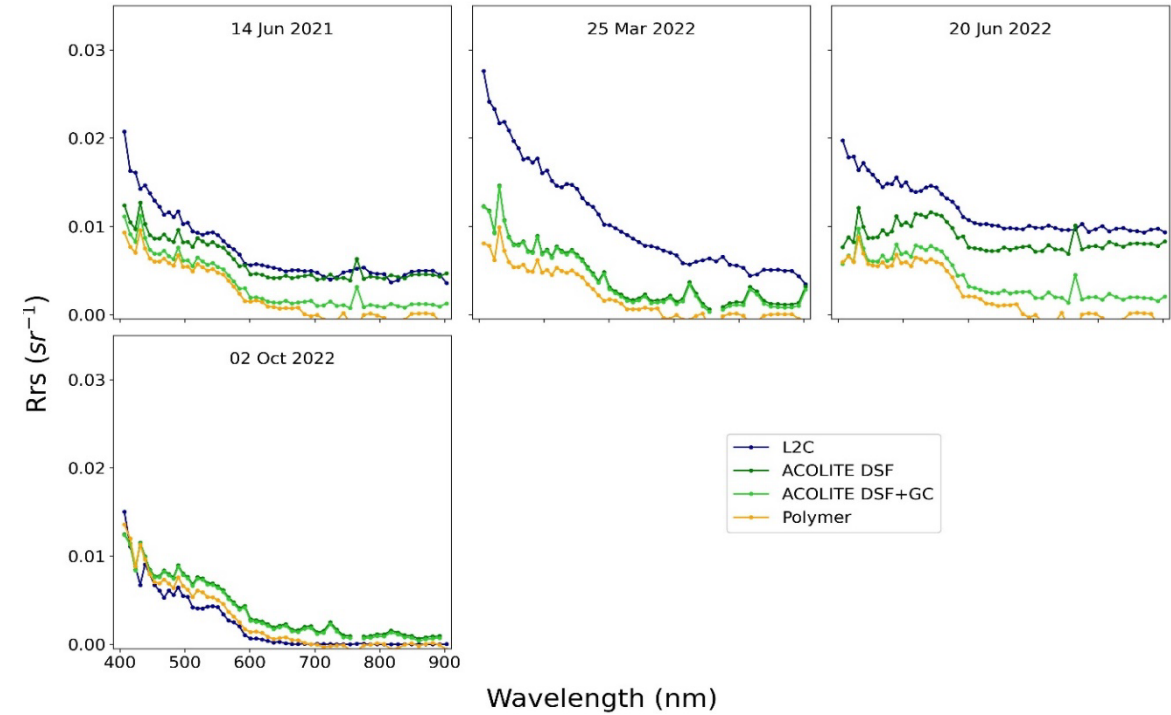


Figure 8. Qualitative comparison of  $R_{rs}$  at L4 buoy. PRISMA  $R_{rs}$  processed using: L2C (blue); ACOLITE with the dark spectrum fitting algorithm (ACOLITE DSF) (green), with the addition of sun-glint correction (ACOLITE DSF + GC) (light green); POLYMER (yellow).

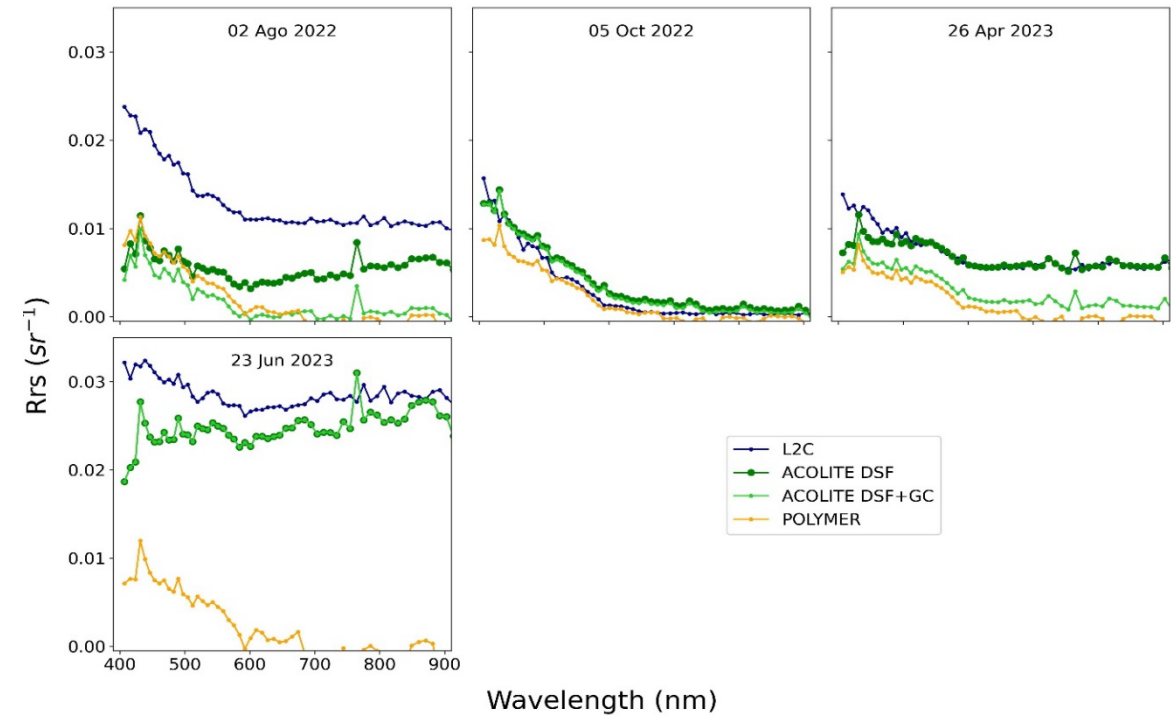


Figure 9. Qualitative comparison of  $R_{rs}$  at Boussole buoy. PRISMA  $R_{rs}$  processed using: L2C (blue); ACOLITE with the dark spectrum fitting algorithm (ACOLITE DSF) (green), with the addition of sun-glint correction (ACOLITE DSF + GC) (light green); POLYMER (yellow).

<b>Project</b>	NECTON No 101081273	<b>Deliverable</b>	4.2
<b>Dissemination</b>	Public	<b>Nature</b>	Report
<b>Date</b>	31 <sup>st</sup> December 2024	<b>Version</b>	1.0

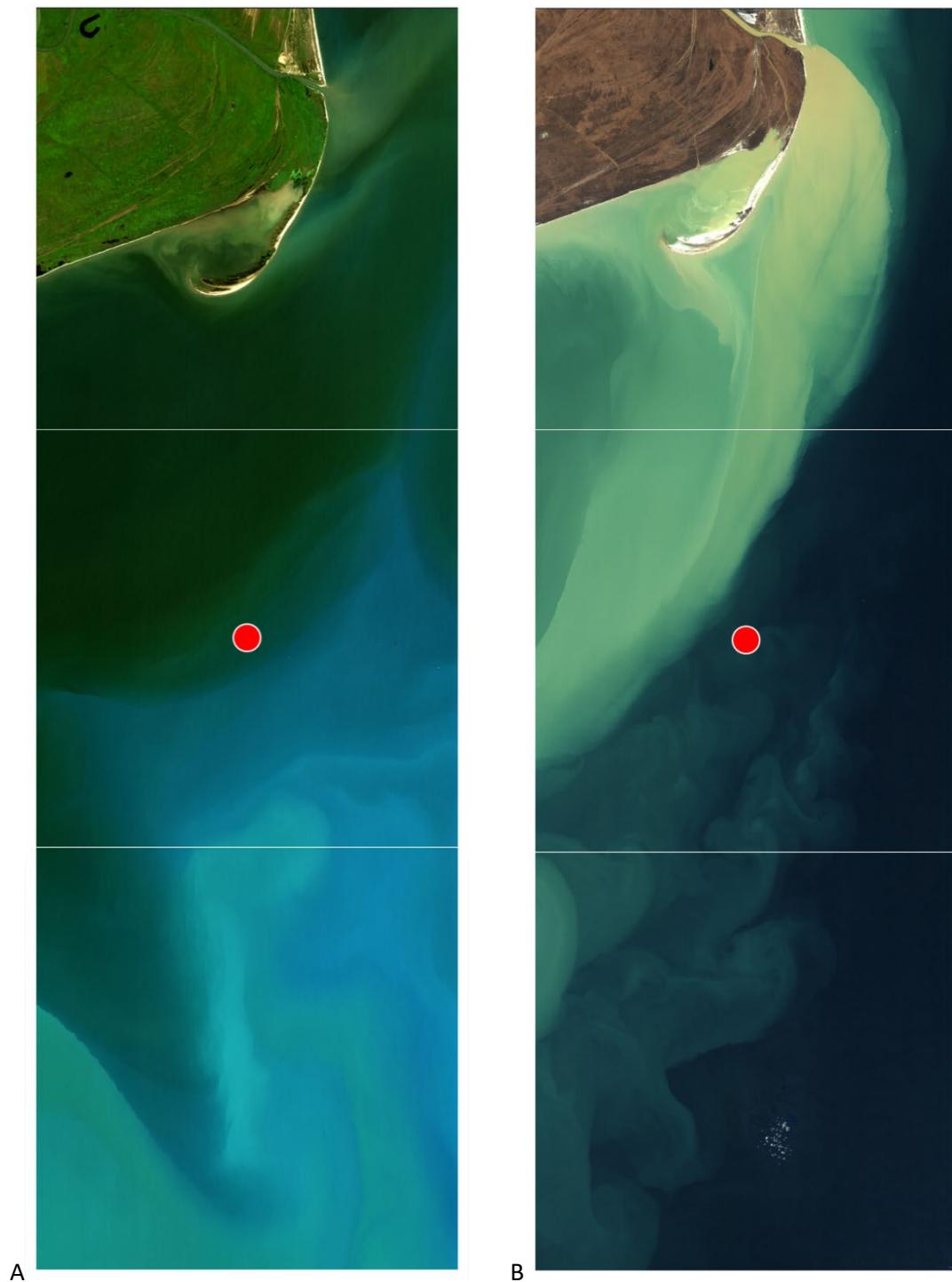


Figure 10. True color PRISMA Stripmap images (30 x 90 km) acquired over the Section-7 Platform, Western Black Sea (red dots). A) on 17<sup>th</sup> June 2022, dark green coastal waters are likely explained by the impact of the Danube River discharge, rich of sediments and organic dissolved matter; turquoise waters are indicative of coccolithophore blooms. B) on 10<sup>th</sup> February 2023, brown-yellowish waters indicate the presence of sediment-rich waters from the Saint George branch of the Danube, affecting the region surrounding Section-7.



<b>Project</b>	NECCTON No 101081273	<b>Deliverable</b>	4.2
<b>Dissemination</b>	Public	<b>Nature</b>	Report
<b>Date</b>	31 <sup>st</sup> December 2024	<b>Version</b>	1.0

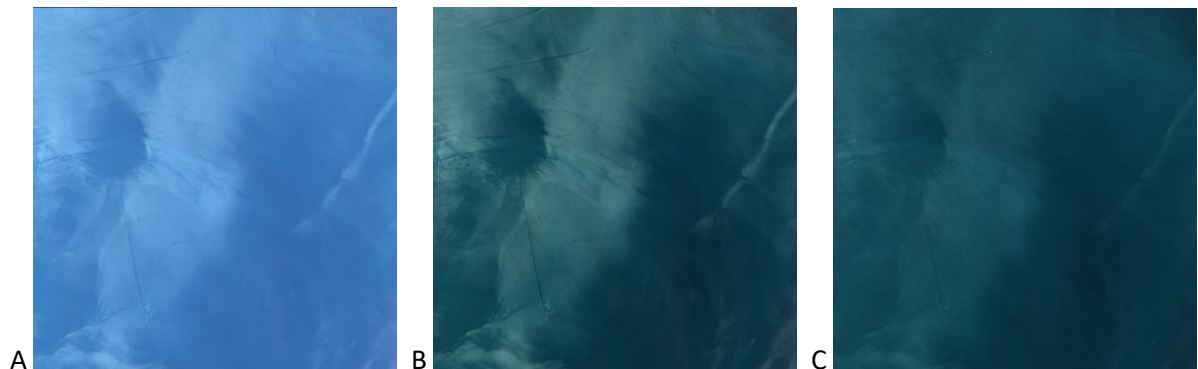


Figure 11. Example of image affected by sun glint and its correction: true color PRISMA image (red 665nm, green 575, blue 483nm) acquired on 31<sup>st</sup> May 2022 over Galata Platform. A) TOA Reflectance; B) ACOLITE DSF; C) ACOLITE DSF + GC.

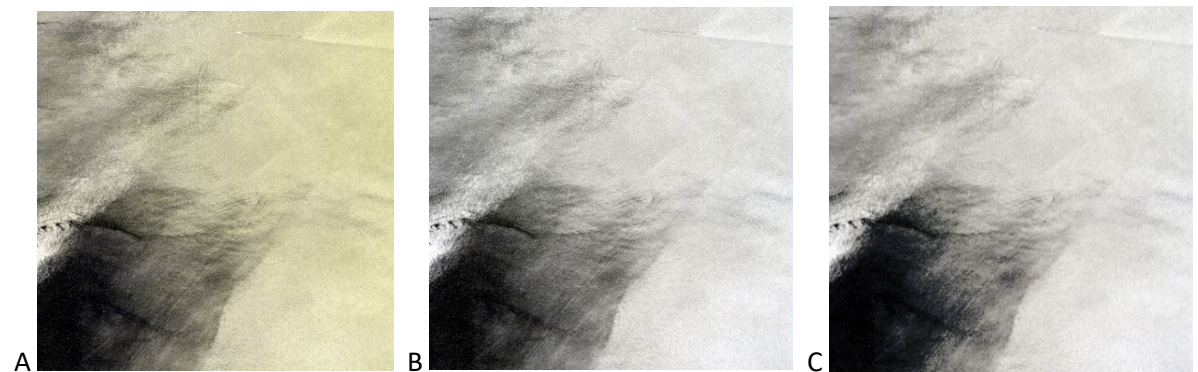
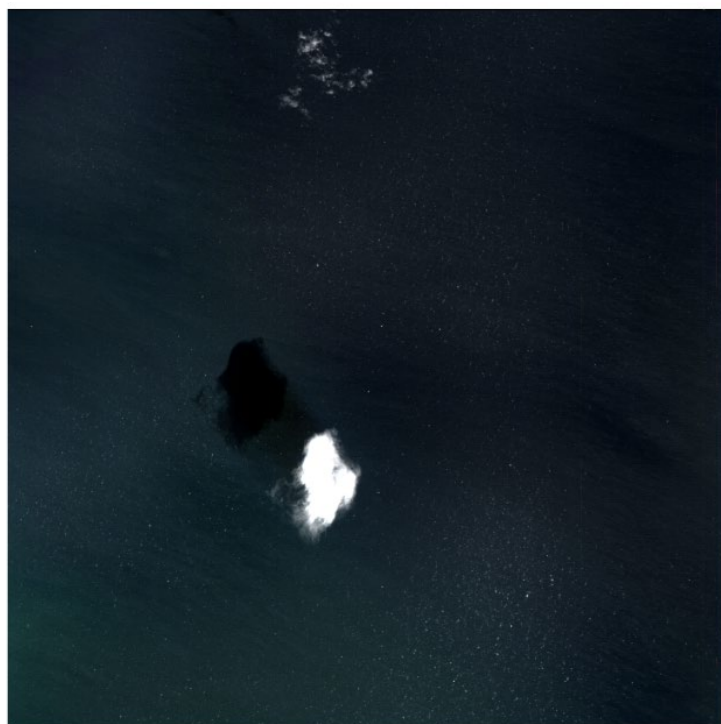


Figure 12. Example of image affected by sun glint and its correction: true color PRISMA image (red 665nm, green 575, blue 483nm) acquired on 17<sup>th</sup> June 2022 over Boussole. A) TOA Reflectance; B) ACOLITE DSF; C) ACOLITE DSF + GC.

<b>Project</b>	NECTON No 101081273	<b>Deliverable</b>	4.2
<b>Dissemination</b>	Public	<b>Nature</b>	Report
<b>Date</b>	31 <sup>st</sup> December 2024	<b>Version</b>	1.0



A



B

Figure 13. Examples of an image with high wind speed (about 9 m/s), where noise due to whitecaps and glint scattering locally affects water reflectance: true color PRISMA images acquired on 11<sup>th</sup> March 2024 over Casablanca Platform. A) TOA Reflectance; B) ACOLITE DSF.

<b>Project</b>	NECCON No 101081273	<b>Deliverable</b>	4.2
<b>Dissemination</b>	Public	<b>Nature</b>	Report
<b>Date</b>	31 <sup>st</sup> December 2024	<b>Version</b>	1.0

Comparison of the median of the match-up spectra from AERONET-OC and from PRISMA (with the dataset variability highlighted by the first and third quartiles) are displayed in Figure 14 for each site and for each AC processor. For all the sites, the spectral shape of POLYMER is the most consistent with the *in situ* data. The median spectra of L2C and ACOLITE tend to systematically overestimate in situ data, especially in the blue (400–500 nm) and NIR (800–900 nm) parts of the spectra. In general, differences increased towards the shorter wavelengths.

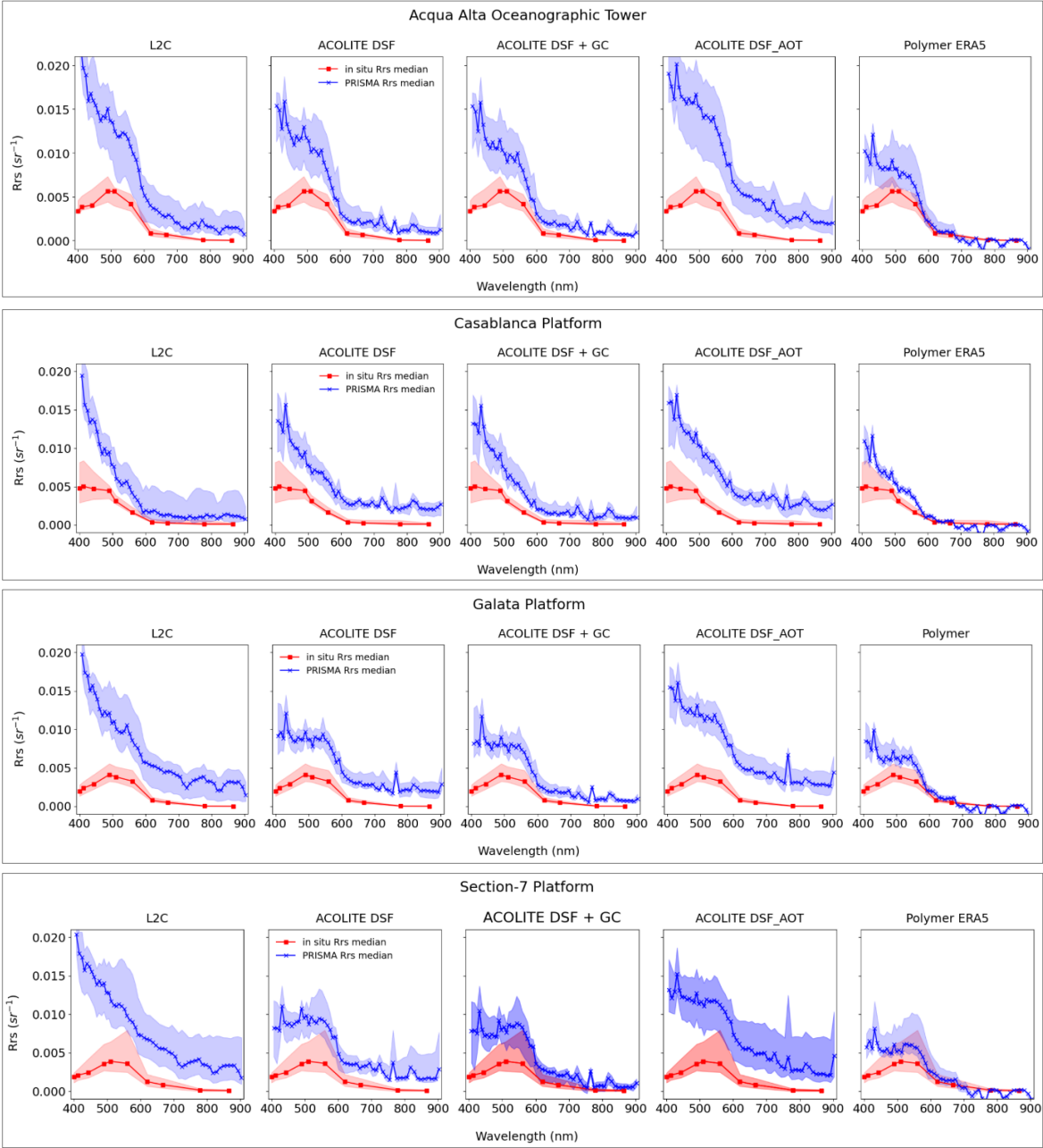


Figure 14. Plots of the median spectra of AERONET-OC (in red) and PRISMA (in blue) for the different atmospheric correction algorithms and for each site. The shadowed areas indicate the distance between the first and third quartiles.

<b>Project</b>	NECCON No 101081273	<b>Deliverable</b>	4.2
<b>Dissemination</b>	Public	<b>Nature</b>	Report
<b>Date</b>	31 <sup>st</sup> December 2024	<b>Version</b>	1.0

## 7.2 Quantitative analysis

The first step of the quantitative analysis of satellite and *in situ* data was the spectral resampling of the PRISMA bands in the range 406.99 – 892 nm to the nine AERONET-OC bands. Both instruments' central bands and bandwidths are listed in Table 5.

Table 5. PRISMA and AERONET-OC band setting. In red the AERONET-OC bands, on which the PRISMA bands were spectrally resampled.

PRISMA		AERONET-OC	
Central $\lambda$	Full width at half maximum	Central $\lambda$	Full width at half maximum
406.993	11.352		
415.839	10.377	412	10
423.785	9.751		
438.657	9.226		
446.015	9.196	443	10
453.389	9.124		
460.732	9.059		
468.098	8.92		
475.319	8.915		
482.548	8.908	490	10
497.059	9.206		
504.512	9.293	510	10
519.544	9.507		
527.305	9.641		
535.053	9.67		
542.885	9.795		
550.915	10.018		
559.020	10.06	560	10
567.206	10.174		
575.487	10.313		
583.844	10.396		
601.014	10.827		
609.958	10.924		
618.712	11.072	620	10
627.778	11.22		
636.676	11.143		
645.964	11.548		
655.419	11.633		
664.894	11.718	667	10
674.464	11.839		
684.137	11.979		
694.128	12.036		
703.737	11.982		
713.727	12.482		
733.955	12.419		
744.150	12.565		
754.470	12.628		
775.273	12.744	779	10
785.660	12.764		
796.127	12.854		
806.711	12.948		
817.311	12.956		
827.919	12.988		
838.527	13.009		
849.210	13.088		
859.973	13.146		
870.743	13.171	865	10
881.456	13.043		
892.081	13.106		



<b>Project</b>	NECCON No 101081273	<b>Deliverable</b>	4.2
<b>Dissemination</b>	Public	<b>Nature</b>	Report
<b>Date</b>	31 <sup>st</sup> December 2024	<b>Version</b>	1.0

The procedure was performed using ENVI® 5.7 software (NV5 Geospatial Solutions, Inc.). Notice that some PRISMA bands (431, 489, 512, 592, 723, 764 and 902 nm) were previously discarded after the qualitative analyses described in the previous paragraph.

After the spectral resampling, all the atmospherically corrected PRISMA data were aggregated by test site and analysed with the corresponding *in situ* AERONET-OC data. The results are shown in Figure 15 and the statistical descriptors are listed in Table 6. The results highlight the performances of the atmospheric processors on the data acquired at the test sites.

The data corrected with POLYMER have the highest coefficient of determination and the lower RMSD and MAD on the AAOT, Galata and Section-7 Platforms. Only at Casablanca, ACOLITE with glint correction shows better results than POLYMER. The L2C processor data have coefficient of determination lower than 0.5 in two sites. As the coefficient of determination describes how well observed data are replicated by the linear model, these values show that the L2C processor can explain less than 50% of the variations in the remote sensing reflectance measured *in situ*. In other words, it has a low to weak predictive capability. This conclusion is supported by both the Root Mean Square Difference (RMSD) and Mean Absolute Difference (MAD) values for L2C; the calculated values are high, the highest on three sites out of four, meaning that on these sites the values calculated by the L2C processor are the most distant from the measured values. The best agreement of L2C is found at Casablanca. This confirms the weak atmospheric correction capability of L2C processor on clear coastal and marine waters.

Figure 15 allows also to evaluate the three ACOLITE products and compare their performances. The results show that the performances of the ACOLITE DSF algorithm on the AAOT and on the Casablanca Platform are higher when the glint correction is included. On the Section-7 Platform data, the results obtained with and without glint correction are similar; while the correlation coefficient is slightly lower with the glint correction, the Root Mean Square Difference and Mean Absolute Difference are slightly higher. Only on Galata Platform data the glint correction leads to poorer prediction capabilities. The graph demonstrates also that ACOLITE AOT has the weakest statistical correlation with *in situ* data, together with the L2C product. The AOT product has been discarded from the data set for subsequent investigations, while L2C products, being the standard PRISMA product, have been included in the following analysis.

ACOLITE and POLYMER were primarily designed for processing multispectral images for aquatic remote sensing applications, and they were modified for processing hyperspectral PRISMA images. They performed satisfactorily and, for ACOLITE, a further improvement is given by the correction of sun glint, taking advantage of the available processing options tailored for aquatic environments.

Project	NECTON No 101081273	Deliverable	4.2
Dissemination	Public	Nature	Report
Date	31 <sup>st</sup> December 2024	Version	1.0

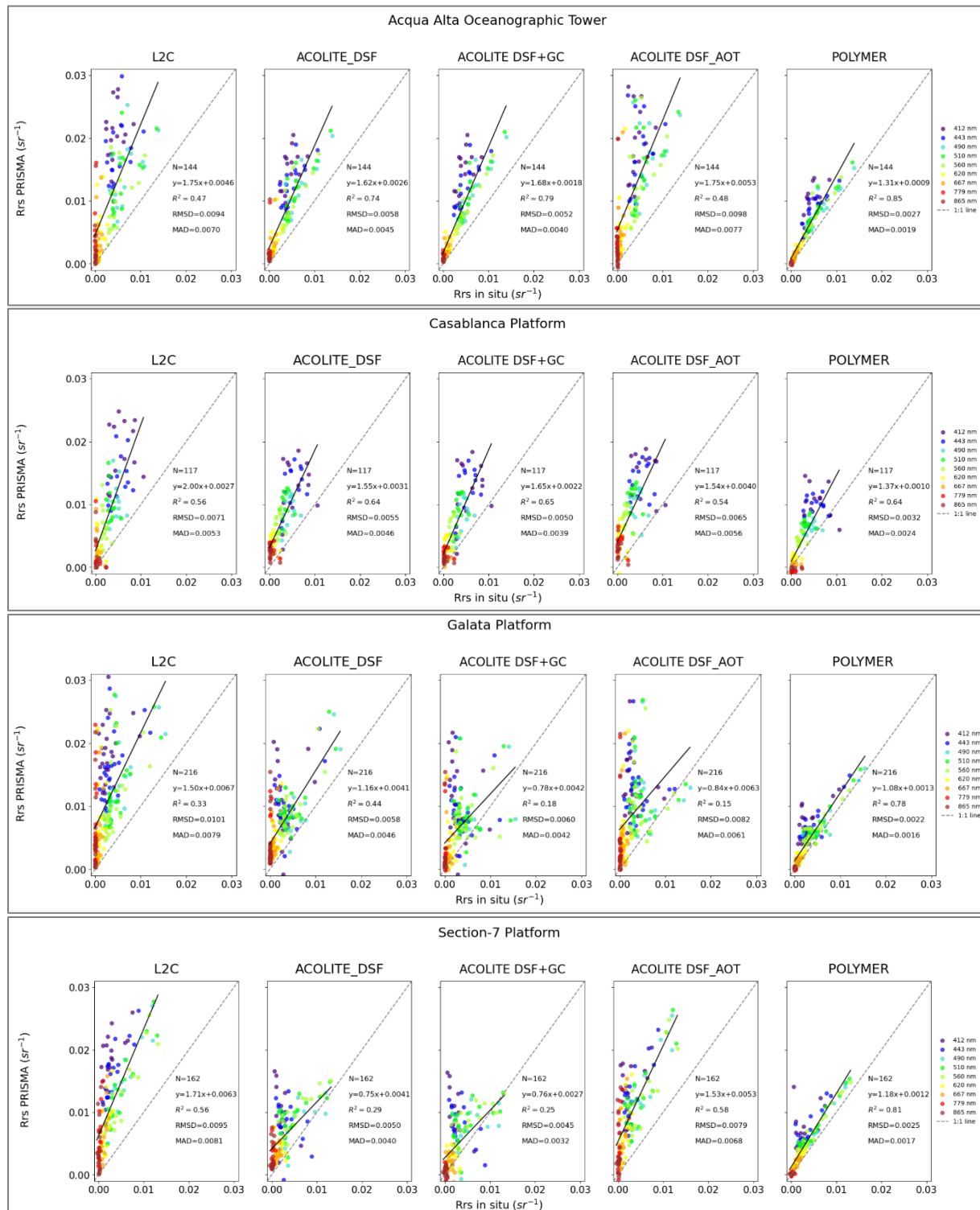


Figure 15. Scatterplots of *in situ* Rrs versus PRISMA Rrs at each test site. Each graph displays the metrics obtained testing a linear regression between the datasets. N represents the number of match-ups at each region. Black solid line is the best-fit linear regression. Grey dashed line is the 1:1 line.

<b>Project</b>	NECCON No 101081273	<b>Deliverable</b>	4.2
<b>Dissemination</b>	Public	<b>Nature</b>	Report
<b>Date</b>	31 <sup>st</sup> December 2024	<b>Version</b>	1.0

Table 6. Descriptive statistics and error metrics for each atmospheric correction algorithm versus *in situ* data, calculated for each site in the 412 – 865 nm range.

	<b>Number of samples (N)</b>	<b>Atmospheric correction method</b>	<b>Coefficient of Determination (R<sup>2</sup>)</b>	<b>Root Mean Squared Difference (RMSD)</b>	<b>Mean Absolute Difference (MAD)</b>
<b>AAOT</b>	144	L2C	0.47	0.0071	0.0070
		ACOLITE DSF	0.74	0.0058	0.0045
		ACOLITE DSF+GC	0.79	0.0052	0.0040
		ACOLITE AOT	0.48	0.0098	0.0077
		POLYMER	0.85	0.0027	0.0019
<b>Casablanca</b>	117	L2C	0.56	0.0071	0.0053
		ACOLITE DSF	0.64	0.0055	0.0046
		ACOLITE DSF+GC	0.65	0.0050	0.0039
		ACOLITE AOT	0.54	0.0065	0.0056
		POLYMER	0.64	0.0032	0.0024
<b>Galata</b>	216	L2C	0.33	0.0101	0.0079
		ACOLITE DSF	0.44	0.0058	0.0046
		ACOLITE DSF+GC	0.18	0.0060	0.0042
		ACOLITE AOT	0.15	0.0082	0.0061
		POLYMER	0.78	0.0022	0.0016
<b>Section-7 Platform</b>	162	L2C	0.56	0.0095	0.0081
		ACOLITE DSF	0.29	0.0050	0.0040
		ACOLITE DSF+GC	0.25	0.0045	0.0032
		ACOLITE AOT	0.58	0.0079	0.0068
		POLYMER	0.81	0.0025	0.0017

Figure 16 shows the Spectral Angle (SA) between PRISMA and *in situ* spectra. The Spectral Angle is a measure of similarity between two spectra in terms of shape, treating them as vectors in a space with dimensionality equal to the number of bands. The smaller the angle, the closer the match. The Spectral Angles were calculated in degrees for better visual interpretation; they are aggregated for all the match ups for each site and for the four AC processors. The Spectral Angles calculated between POLYMER and AERONET-OC data are the smallest at AAOT and Section-7 Platform, suggesting that POLYMER best reproduced the spectral shape of *in situ* data. At Galata and Casablanca Platforms, the spectral angles of POLYMER and ACOLITE products are similar, but

<b>Project</b>	NECCTON No 101081273	<b>Deliverable</b>	4.2
<b>Dissemination</b>	Public	<b>Nature</b>	Report
<b>Date</b>	31 <sup>st</sup> December 2024	<b>Version</b>	1.0

ACOLITE + GC achieves the lowest median. L2C data has the larger Spectral Angles among the AC processors. At Galata and Section-7, wide ranges of Spectral Angles for ACOLITE and ACOLITE + GC indicate that their performances can vary depending on sea state conditions and water quality.

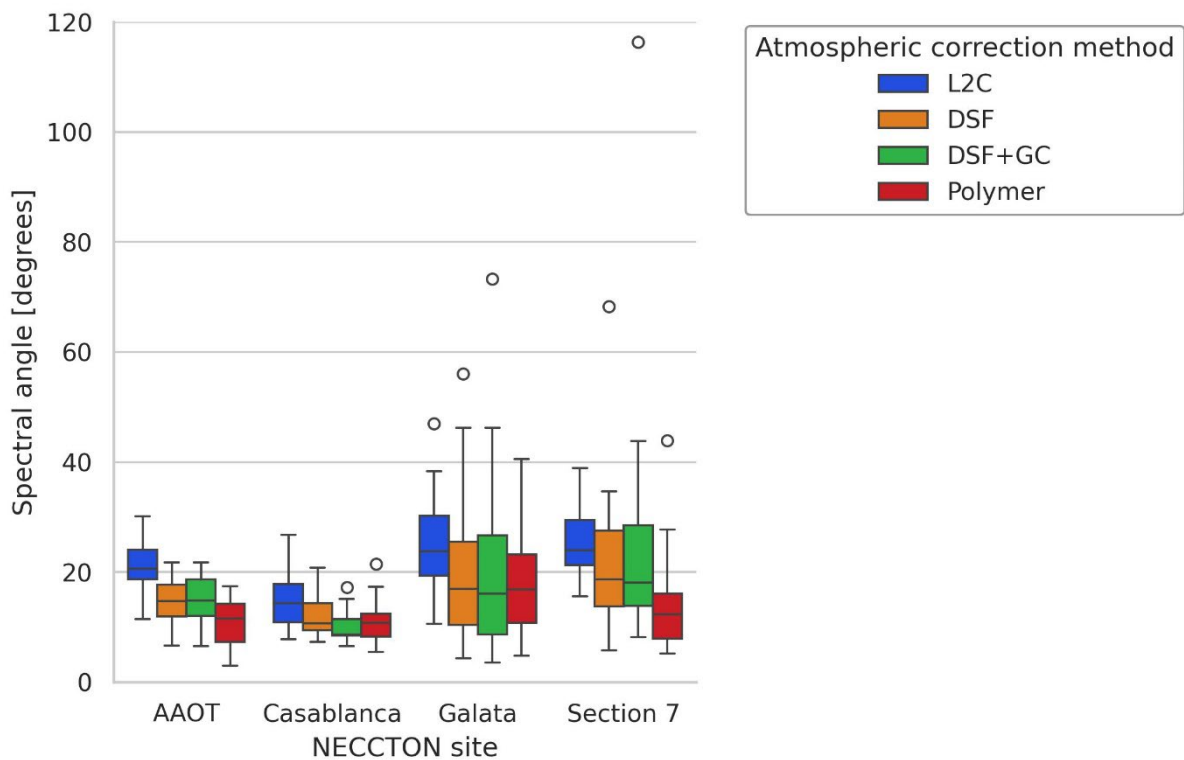


Figure 166. Spectral Angle between AERONET-OC *in situ* data and spectrally resampled PRISMA data, at each test site. The data shown in the figures is aggregated according to atmospheric correction method. Solid line shows the median. Box limits indicate the 1st quartile and the 3rd quartile, whiskers extend 1.5 times the interquartile range. Outliers are indicated by white circles. The number of samples is 16 at AAOT, 13 at Casablanca, 24 at Galata and 18 at Section-7 Platforms.

<b>Project</b>	NECCON No 101081273	<b>Deliverable</b>	4.2
<b>Dissemination</b>	Public	<b>Nature</b>	Report
<b>Date</b>	31 <sup>st</sup> December 2024	<b>Version</b>	1.0

Figure 17 shows the scatterplots of data for each center-wavelength of the nine AERONET-OC bands in the range 412 to 865 nm. The best linear fit is shown for each AC method (excluding ACOLITE AOT). It is relevant to notice that the variability of *in situ* data at 779 and 865 nm is very limited; PRISMA data appear to be almost uncorrelated with them, and the best linear fits are strongly influenced by data outliers.

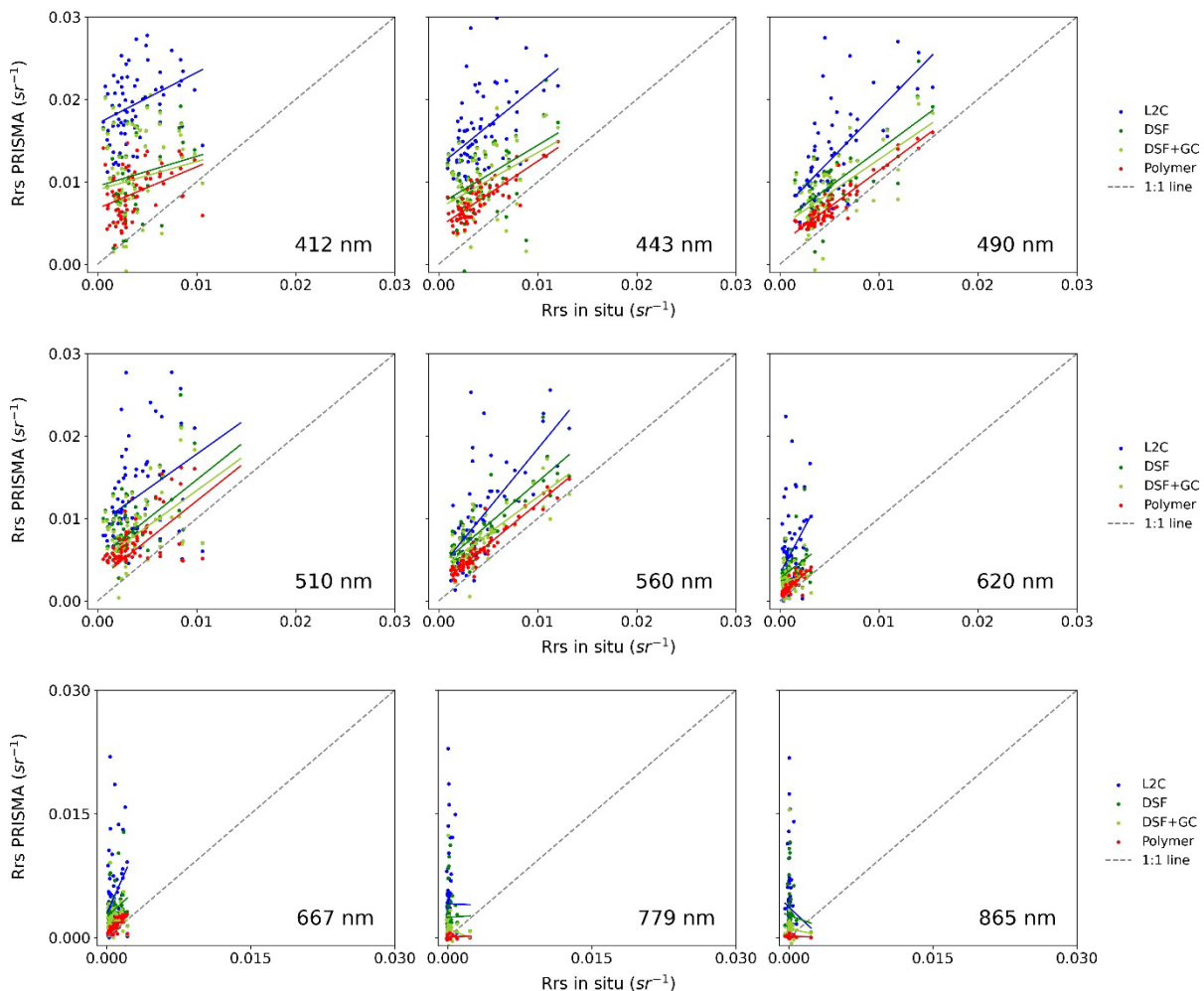


Figure 17. Scatterplots of the AERONET-OC *in situ* data and the atmospherically corrected, spectrally resampled PRISMA data, aggregated by spectral band (N=71). The coloured lines show the best linear fit for each atmospheric correction method. The grey dashed line is the 1:1 line.

To quantify these observations,  $R^2$  of the linear correlations between AERONET-OC *in situ* data and each atmospherically corrected, spectrally resampled PRISMA data has been calculated as a function of wavelength in the 412 – 865 nm range (Figure 18), on the complete set of data for all sites. Figure 19 shows that the dataset of POLYMER has a very weak coefficient of determination at 412 nm ( $<0.2$ ). Their  $R^2$  values are greater than 0.6 at 443 nm and 620 nm, and slightly lower at 667 nm. This

<b>Project</b>	NECCTON No 101081273	<b>Deliverable</b>	4.2
<b>Dissemination</b>	Public	<b>Nature</b>	Report
<b>Date</b>	31 <sup>st</sup> December 2024	<b>Version</b>	1.0

indicates a good correlation between the two data sets at these wavelengths. In the 490 – 560 nm range,  $R^2$  is greater than 0.8; in particular, it reaches 0.9 at 510 nm and 560 nm, showing a very strong correlation in these bands. At the longest wavelengths (779 and 865 nm) the values of  $R^2$  drop to almost zero, confirming that the image values are uncorrelated with *in situ* data. ACOLITE produces data with a good correlation with AERONET-OC data, albeit lower than POLYMER, at 560 nm, while the correlation at 490 and 510 nm is 0.5. At 412, 620 and 667 nm the results show a very weak correlation. The values of  $R^2$  obtained for DSF+GC are slightly lower than those obtained without the glint correction in all the 412 – 667 nm range. At 779 and 865 nm the values of  $R^2$  are approximately zero, both with and without glint correction. Finally, L2C products are confirmed to have a weak correlation at their best, i.e. 0.5 at 560 nm, and very weak at all the other wavelengths. At 779 and 865 the correlation is almost zero.

All atmospherically corrected PRISMA data appear to be uncorrelated to *in situ* data at 779 and 865 nm. So, these bands have been discarded and further quantitative analyses have been carried out uniquely on the six AERONET-OC bands in the 412 to 667 nm range.

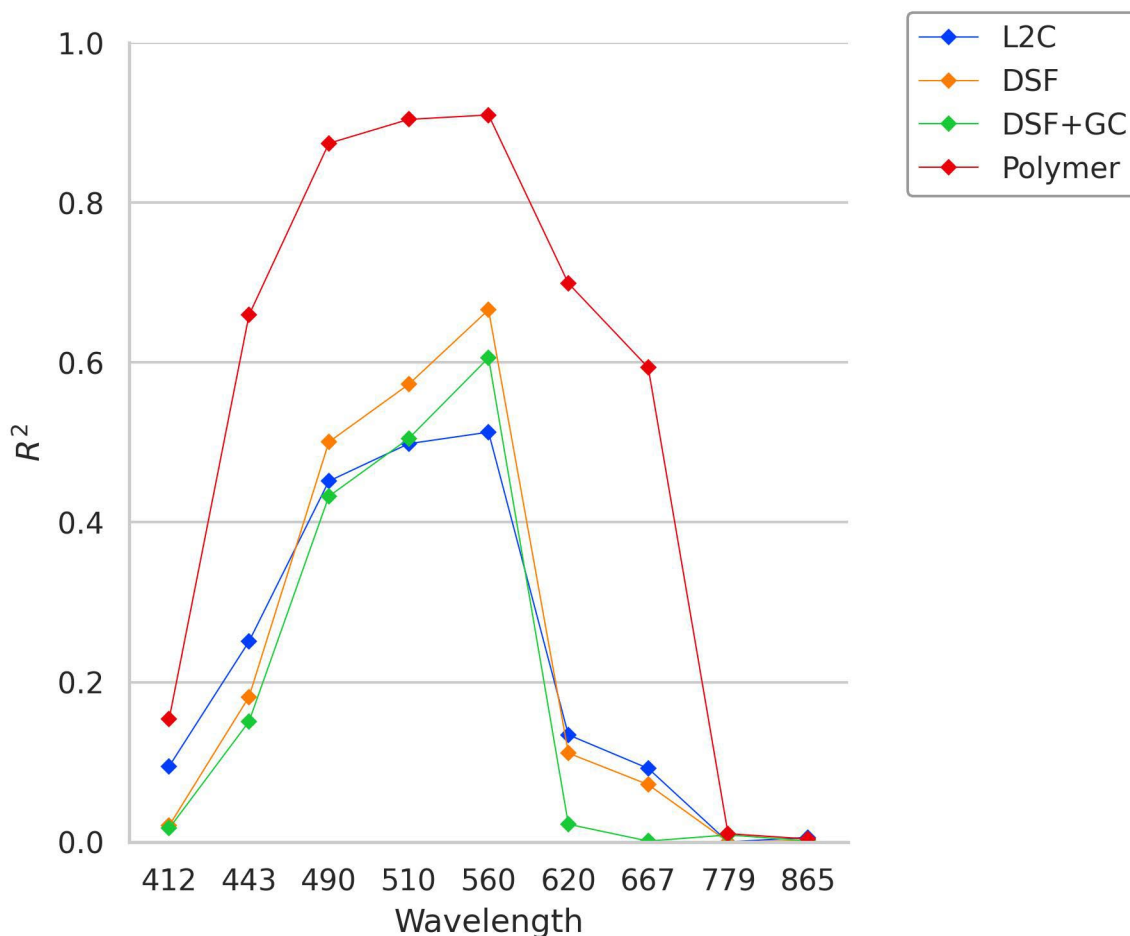


Figure 18. Coefficient of determination ( $R^2$ ) calculated between AERONET-OC data and PRISMA data, by atmospheric correction method, as a function of wavelength. The total number of samples is 71.

<b>Project</b>	NECCON No 101081273	<b>Deliverable</b>	4.2
<b>Dissemination</b>	Public	<b>Nature</b>	Report
<b>Date</b>	31 <sup>st</sup> December 2024	<b>Version</b>	1.0

Table 7. Descriptive statistics and error metrics for each atmospheric correction algorithm versus *in situ* data, calculated for wavelength in the 412 – 667 nm range. The number of samples is 71.

Atmospheric correction method	Center-wavelength	Coefficient of Determination (R <sup>2</sup> )	Root Mean Squared Difference (RMSD)	Mean Absolute Difference (MAD)	Mean Absolute Percent Difference (MAPD)
L2C	412	0.09	0.0162	0.0156	641
	443	0.25	0.0125	0.0118	383
	490	0.45	0.0086	0.0076	175
	510	0.50	0.0085	0.0075	181
	560	0.51	0.0071	0.0058	169
	620	0.13	0.0063	0.0047	619
	667	0.09	0.0060	0.0041	877
ACOLITE DSF	412	0.02	0.0094	0.0082	383
	443	0.18	0.0071	0.0065	233
	490	0.50	0.0051	0.0045	118
	510	0.57	0.0055	0.0049	133
	560	0.67	0.0047	0.0043	141
	620	0.11	0.0033	0.0027	407
	667	0.07	0.0032	0.0025	604
ACOLITE DSF+GC	412	0.02	0.0091	0.0079	37
	443	0.15	0.0067	0.0061	219
	490	0.43	0.0045	0.0040	104
	510	0.50	0.0048	0.0042	116
	560	0.61	0.0038	0.0033	114
	620	0.02	0.0022	0.0018	279
	667	0.00	0.0020	0.0015	374
POLYMER	412	0.15	0.0057	0.0050	236
	443	0.66	0.0039	0.0037	129
	490	0.87	0.0021	0.0019	50
	510	0.90	0.0025	0.0023	63
	560	0.91	0.0020	0.0019	62
	620	0.70	0.0089	0.0008	106
	667	0.59	0.0006	0.0005	1057236

The Coefficient of Determination and the other descriptive statistics, calculated for each AC method as a function of wavelength, are shown in Table 7.

The Root Mean Squared Difference (RMSD) measures the quadratic mean of the differences between *in situ* (AERONET-OC) data and the atmospherically corrected, spectrally resampled PRISMA values. It allows us to compare forecasting errors of the different processors on the various test sites. RMSD is expressed in the same units as the data; the minimum theoretical value of this parameter is 0, and it can assume positive values up to  $\infty$ . Values nearer to zero indicate smaller

<b>Project</b>	NECCON No 101081273	<b>Deliverable</b>	4.2
<b>Dissemination</b>	Public	<b>Nature</b>	Report
<b>Date</b>	31 <sup>st</sup> December 2024	<b>Version</b>	1.0

differences between the *in situ* values and the values obtained with the atmospheric correction of satellite sensor data. Regardless of the test site, the RMSD values are highest at the smaller wavelengths; in this range, the differences between satellite data and ground data reach the highest values. The differences are smaller at the longer wavelengths, since both satellite and ground data values tend zero. In general, this statistical descriptor shows that POLYMER has the lowest RMSD for all wavelengths. Data corrected with ACOLITE DSF and DSF+GC have approximately the same RMSD and L2C data show the highest values.

The Mean Absolute Difference (MAD) is the average of the absolute values of the differences between AERONET-OC *in situ* data and atmospherically corrected, spectrally resampled PRISMA data. It indicates to what degree the atmospherically corrected data depart from *in situ* data, on average and regardless of the sign of the error. MAD is expressed in the same units as the data; the lower the MAD, the more accurate the atmospheric correction is. In this context, the range of MAD data values is quite the same as RMSD, as expected. MAD values show that on average, POLYMER data has the lowest absolute differences from the measured values, and L2C the highest.

The Mean Absolute Percentage Difference (MAPD) is derived from the MAD to express differences in percentage, theoretically helping in conceptualizing the results. Low percentages indicate high processing accuracy. It must be noticed that for atmospherically corrected values that are lower than *in situ* data the higher value of MAPD is 100%, but for corrected data higher than *in situ* data there is no upper limit to MAPD. In fact, MAPD values are very high at the shorter wavelengths, where the atmospherically corrected data range from twice to six times those recorded by AERONET. Besides, if the atmospherically corrected data are close to zero, as happens at the longer wavelength, the values of MAPD grow to infinity. In this context, these characteristics strongly influence the values of MAPD, that grow up to 1100% at the longer wavelengths where the PRISMA and AERONET values are almost zero. Thus, in this context the interpretation of MAPD data is less intuitive. In general, it shows that POLYMER values have the lowest uncertainties and the best performances among the AC processors.

In conclusion, the quantitative analysis has confirmed that the standard PRISMA L2C product is less adequate over coastal and open sea waters: these uncertainties could be due to the inaccurate estimation of AOT or the aerosol model used in the AC procedure. The results demonstrate that POLYMER is the best processor for the atmospheric correction of PRISMA imagery in oligo-mesotrophic waters, and that ACOLITE is the second best. Both processors overestimate remote sensing reflectance at the shorter wavelengths, while a very good agreement with *in situ* data has been proved for POLYMER products in the 443 to 620 range.

Finally, it is important to notice that on November 2022, a recalibration of the VNIR and SWIR channels of PRISMA L1 data was made for improving the radiometric quality of the products over terrestrial targets. This caused quite negative effects on the atmospheric correction over clear water targets if we compare the results of this study with the ones in Braga et al. (2022) for AAOT site, where the performances of L2C and ACOLITE are quite better.



<b>Project</b>	NECCON No 101081273	<b>Deliverable</b>	4.2
<b>Dissemination</b>	Public	<b>Nature</b>	Report
<b>Date</b>	31 <sup>st</sup> December 2024	<b>Version</b>	1.0

## 8. Transferability of the validation approach to future hyperspectral missions

Several spaceborne missions provide unique observations, depending on their spatial, temporal and radiometric resolution, that may advance knowledge in different aquatic processes spanning space and time. However, all present and historic hyperspectral missions are regional in scope and only collect imagery from specific targeted locations (Dierssen et al., 2023). Missions like NASA’s PACE, that combines the characteristics of operational ocean color satellites (1-day to 2-day global coverage, wide swath, high sensitivity) with hyperspectral capabilities can offer new opportunities to assess phytoplankton diversity and community composition and global biogeochemical cycling (Figure 19). PACE is the first global ocean hyperspectral mission and collects ocean color imagery over a period of one-to-two days from a sun-synchronous polar orbit. The spacecraft host three instruments, including a hyperspectral imaging radiometer named OCI (Ocean Color Instrument), developed by NASA Goddard Space Flight Center. OCI covers a spectral range that continuously spans from the ultraviolet to near-infrared, with nominal spectral steps of 2.5 nm and average bandwidths of ~5 nm across a spectral range of 340–890 nm. The spatial resolution of OCI imagery is ~1.1 km at nadir with a swath width of 2663 km. Due to the specific optical design, time-delayed integration, lunar, spectral calibrations, and tilt mechanism OCI produces high-quality data over a very high dynamic range of radiances from highly absorbing waters to ecosystems rich in inorganics (Werdell et al., 2019; Cetinic et al., 2024).

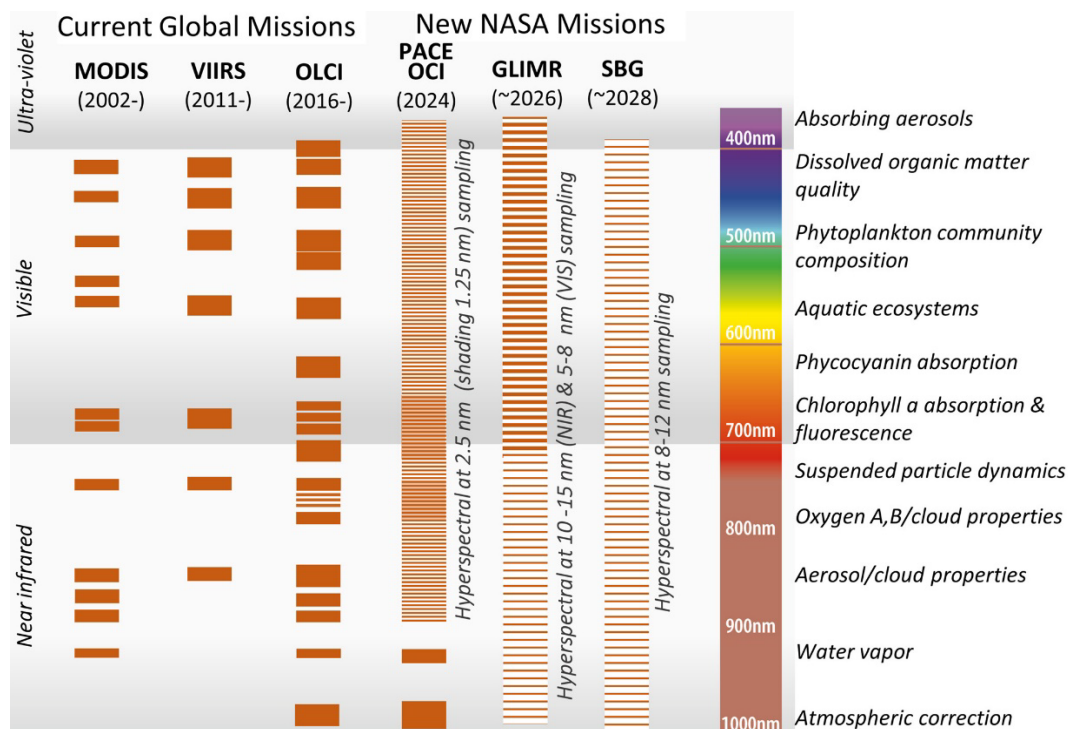


Figure 18. Comparison of the spectral characteristics of the 3 new NASA hyperspectral missions (PACE - launched in 2024, GLIMR and SBG – expected in 2026 and 2028, respectively) compared to the capabilities of current global ocean color sensors. Modified from Dierssen et al. (2023).

<b>Project</b>	NECCON No 101081273	<b>Deliverable</b>	4.2
<b>Dissemination</b>	Public	<b>Nature</b>	Report
<b>Date</b>	31 <sup>st</sup> December 2024	<b>Version</b>	1.0

The match-up procedure applied in this study can be transferred to assess the quality of Rrs of current and future hyperspectral Earth Observation missions, but this requires the availability of *in situ* hyperspectral fiducial reference measurements for the product assessment and harmonization, through robust statistical analyses, providing further information on the performance under different atmospheric conditions and across various optical water types. The availability of *in situ* hyperspectral measurements, such as those provided by WATERHYPERNET, is particularly important in view of the increase in availability of spaceborne hyperspectral data in the near future.

The “very preliminary” results of the methodology implemented in González Vilas et al. (2024) in the framework of HYPERNETS-POP (ESA) and now adapted to PACE, using the data acquired by HYPSTAR at AAOT, are shown in Figure 20. In the period from the 5<sup>th</sup> of March to the 31<sup>st</sup> of August 2024 (180 days), 53 valid match-ups between PACE/OCI imagery and HYPSTAR dataset are available (quality checks based on 2 hours-time window, *in situ* quality control, satellite quality control). The last version of standard products (PACE OCI Level-2 Surface Reflectance, Version 2.0) was used (NASA Ocean Biology Processing Group, 2024).

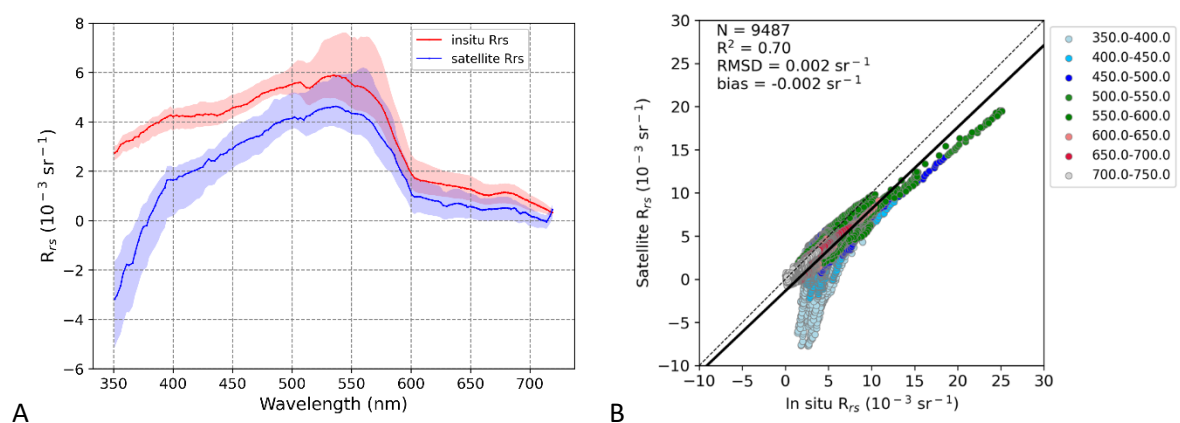


Figure 19. PACE/OCI versus HYPSTAR *in situ* data at the AAOT (53 match-ups): A) the qualitative spectral comparison (median values in blue for OCI data and red for HYPSTAR data; shadowed areas indicate the interquartile ranges) and B) the quantitative comparison with statistics (the black line shows the best linear fit; the black dashed line is the 1:1 line) on the right. N represents the total number of match-up points.

An overall underestimation of PACE/OCI Rrs is evident, probably due to the wide ROI used (25 x 25 pixels) which includes coastal-to-open sea waters. Noticeable is the low and partially negative signal in the range between 350 and 400 nm in PACE, probably due to the overcorrection of aerosol effects in this part of the Rrs spectra, reflecting the challenging estimation of atmospheric path reflectance in the ultraviolet spectral region for the offshore clear waters of northern Adriatic Sea.

<b>Project</b>	NECCTON No 101081273	<b>Deliverable</b>	4.2
<b>Dissemination</b>	Public	<b>Nature</b>	Report
<b>Date</b>	31 <sup>st</sup> December 2024	<b>Version</b>	1.0

## 9. PRISMA data stream as validation and assimilation tool for biogeochemical models

Traditionally, biogeochemical models use a simple Beer-Lambert formula to describe the propagation of photosynthetically available radiation (PAR) along the water column, which decays exponentially due to attenuation. In parallel, in recent years, several biogeochemical models have begun to resolve spectral (and partly also directional) light propagation, to simulate light absorption, as well as photon scattering and backscattering, and to directly model the remote sensing reflectance ( $R_{rs}$ ) (Dutkiewitz et al., 2015; Gregg and Rousseaux, 2016, 2017; Baird et al., 2016; Skakala et al., 2020, 2022; Lazzari et al., 2021; Cahill et al., 2023; Maggiorano et al., 2024). Within NECCTON, several Monitoring and Forecasting Centres (MFCs) are developing and implementing improved bio-optical simulation capabilities in the different regions monitored by Marine Copernicus Services such as the Baltic Sea, the Black Sea, the Mediterranean Sea and the North-West European shelf areas. These improvements in modelling algorithms are in line with the systematic increase in data streams received from multispectral (Global Monitoring for Environment and Security - GMES-Sentinel-3) and hyperspectral (*PRecursore IperSpettrale della Missione Applicativa - PRISMA*; Plankton, Aerosol, Clouds, Ocean Ecosystem - PACE) satellite ocean color sensors.

The  $R_{rs}$  data stream is relevant for the coupled biogeochemistry – optical model validation, to implement skill metrics based on satellite and modelled  $R_{rs}$  (Álvarez et al., in prep), and to perform data assimilation of reflectance. The hypothesis is that assimilating reflectance into the model might outperform chlorophyll assimilation in optically complex (mostly coastal) waters, where chlorophyll retrieval algorithms might have more limited skill. An example of proposed validation and assimilation architecture is shown in Figure 21 (Lazzari et al., 2024).

As an example of application, we consider the site of AAOT where a version of the FABM prototype developed within NECCTON has been deployed (Álvarez et al., in prep). The simulation period does not cover the exact period of the PRISMA acquisition because the BC data provided by the North Adriatic regional model (Bruschi et al., 2021) and required for the correct functioning of the 1D setup in the coastal site of AAOT were not available for the time window. The qualitative comparison is therefore carried out by comparing the seasonal spectral signature of  $R_{rs}$  for winter and summer data (Figure 22).

The model was calibrated with the six waveband  $R_{rs}$  satellite product from the Copernicus Marine Service (OCEANCOLOUR\_MED\_BGC\_L3\_MY\_009\_143 - European Union-Copernicus Marine Service (2022)). As result, during winter, the model is more coherent with the Ocean Colour multi-sensor product (OC\_MULTI) and slightly less with the Ocean Colour OLCI-sensor product (OC\_OLCI). We observe for both winter and summer a tendency of the model to underestimate the PRISMA  $R_{rs}$  in the range of 400 – 500 nm (Figure 22). During summer the model shows intermediate values between PRISMA and CMEMS  $R_{rs}$  products. Above 550 nm, results are always consistent for all the data stream and model output considered.

<b>Project</b>	NECTON No 101081273	<b>Deliverable</b>	4.2
<b>Dissemination</b>	Public	<b>Nature</b>	Report
<b>Date</b>	31 <sup>st</sup> December 2024	<b>Version</b>	1.0

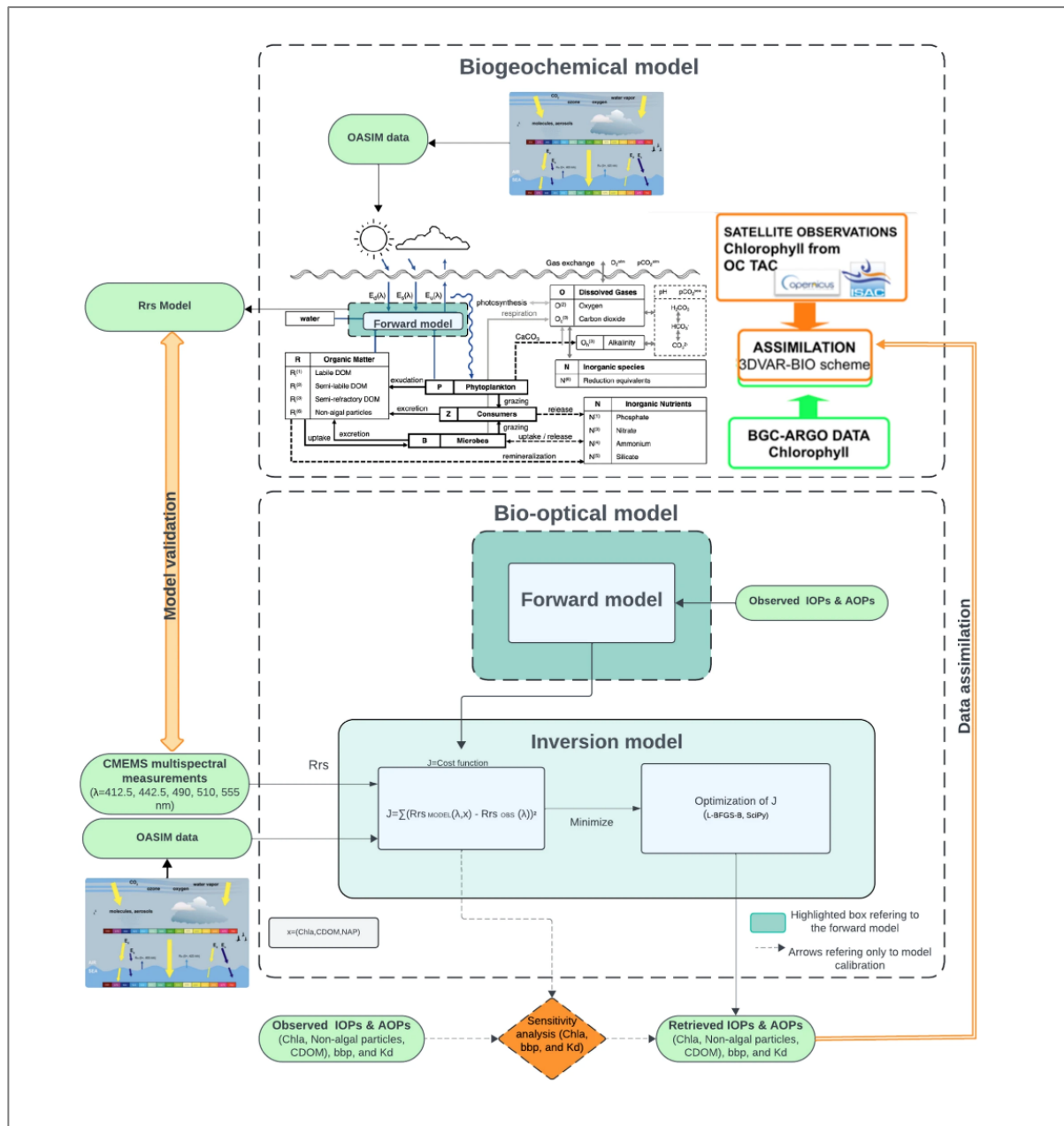


Figure 20. Schematic flowchart of the operational system leveraging Rrs datastreams, with an example application from the Mediterranean Biogeochemical model used within Copernicus MedMFC. The bio-optical model can be used both in forward mode and in for the inversion. The line regarding data assimilation points to applications that will be developed within WP4 and WP5.

<b>Project</b>	NECCTON No 101081273	<b>Deliverable</b>	4.2
<b>Dissemination</b>	Public	<b>Nature</b>	Report
<b>Date</b>	31 <sup>st</sup> December 2024	<b>Version</b>	1.0

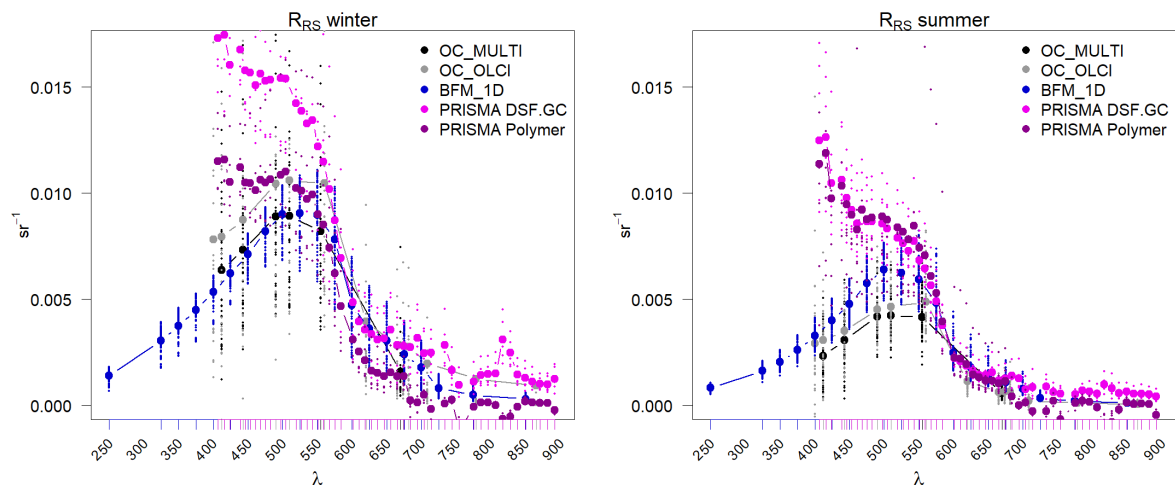


Figure 21. Qualitative comparison of  $R_{rs}$  spectral shapes from the different data streams and modelling output (BFM\_1D) for the AAOT site. Data are aggregated over the same winter and summer seasons. The winter panel shows 5 profiles of PRISMA acquired in the following days "2021-03-09", "2022-03-20", "2022-03-26", "2023-01-28" and "2023-03-03", and their median. The summer panel shows 7 profiles of PRISMA acquired in the following days "2019-07-14", "2020-07-25", "2020-08-29", "2021-08-06", "2021-08-12", "2021-09-10" and "2022-09-10", and their media.

Finally, we see a great potential benefit of using model reanalyses assimilating hyperspectral PRISMA reflectance data, and resolving in detail the optically active biogeochemical tracers, to inform development of more detailed satellite retrieval algorithms for a range of tracers. This can be accomplished e.g. using machine learning/AI.

## 10. Acknowledgments

We would like to thank M. Talone, F. Mélin, B. Bulgarelli, the principal investigators of the AERONET-OC stations, and all colleagues from the H2020/HYPERNETS for WATERHYPERNET data. This study was carried out using PRISMA Products, © of the Italian Space Agency (ASI), delivered under an ASI License to use. The analysis of PACE data was carried out in the context of the HYPERNET-POP project, funded by the European Space Agency (contract n° 4000139081/22/I-EF).

<b>Project</b>	NECCTON No 101081273	<b>Deliverable</b>	4.2
<b>Dissemination</b>	Public	<b>Nature</b>	Report
<b>Date</b>	31 <sup>st</sup> December 2024	<b>Version</b>	1.0

## 11. References

- Álvarez, E., Occhipinti, G., Cossarini, G., Aubry, F. B., Braga, F., Lazzari, P. (2025). The influence of optical scattering by organic and inorganic particles in the reflectance spectra of two contrasting sites of the Mediterranean Sea, in prep.
- Antoine, D., Chami, M., Claustre, H., d'Ortenzio, F., Morel, A., Bécu, G., ... & Adams, D. (2006). BOUSSOLE: A joint CNRS-INSU, ESA, CNES, and NASA ocean color calibration and validation activity (No. Rept-2007-00282-0).
- Antoine, D., Guevel, P., Deste, J. F., Becu, G., Louis, F., Scott, A. J., & Bardey, P. (2008). The “BOUSSOLE” buoy—A new transparent-to-swell taut mooring dedicated to marine optics: Design, tests, and performance at sea. *Journal of Atmospheric and Oceanic Technology*, 25(6), 968-989.
- ASI - Italian Space Agency (2020). PRISMA Products Specification Document, Issue 2.3, Date 12/03/2020. [https://prisma.asi.it/missionselect/docs/PRISMA%20Product%20Specifications\\_Is2\\_3.pdf](https://prisma.asi.it/missionselect/docs/PRISMA%20Product%20Specifications_Is2_3.pdf). (Accessed 27 November, 2024).
- ASI – Italian Space Agency (2021). PRISMA Algorithm Theoretical Basis Document (ATBD), Issue 1, Date 14/12/2021. [https://prisma.asi.it/missionselect/docs/PRISMA%20ATBD\\_v1.pdf](https://prisma.asi.it/missionselect/docs/PRISMA%20ATBD_v1.pdf) (Accessed 27 November, 2024).
- Bailey, S. W., & Werdell, P. J. (2006). A multi-sensor approach for the on-orbit validation of ocean color satellite data products. *Remote sensing of environment*, 102(1-2), 12-23.
- Baird, M. E., Cherukuru, N., Jones, E., Margvelashvili, N., Mongin, M., Oubelkheir, K., Ralph, P. J., Rizwi, F., Robson, B. J., Schroeder, T., Skerratt, J., Steven, A. D. L., & Wild-Allen, K. A. (2016). Remote-sensing reflectance and true colour produced by a coupled hydrodynamic, optical, sediment, biogeochemical model of the Great Barrier Reef, Australia: Comparison with satellite data. *Environmental Modelling & Software*, 78, 79–96.
- Berthon, J. F., Mélin, F., & Zibordi, G. (2008). Ocean colour remote sensing of the optically complex European seas. In *Remote sensing of the European seas* (pp. 35-52). Dordrecht: Springer Netherlands.
- Berthon, J. F., & Zibordi, G. (2004). Bio-optical relationships for the northern Adriatic Sea. *International Journal of Remote Sensing*, 25(7-8), 1527-1532.
- Braga, F., Fabbretto, A., Vanhellefont, Q., Bresciani, M., Giardino, C., Scarpa, G. M., ... & Brando, V. E. (2022). Assessment of PRISMA water reflectance using autonomous hyperspectral radiometry. *ISPRS Journal of Photogrammetry and Remote Sensing*, 192, 99-114.
- Bruschi, A., Lisi, I., De Angelis, R., Querin, S., Cossarini, G., Di Biagio, V., Salon, S., Solidoro, C., Fassina, D., Ancona, S. & Silvestri, C. (2021). Indexes for the assessment of bacterial pollution in bathing waters from point sources: The northern Adriatic Sea CADEAU service. *Journal of Environmental Management*, 293, 112878.

<b>Project</b>	NECCON No 101081273	<b>Deliverable</b>	4.2
<b>Dissemination</b>	Public	<b>Nature</b>	Report
<b>Date</b>	31 <sup>st</sup> December 2024	<b>Version</b>	1.0

- Cahill, B. E., Kowalczyk, P., Kritten, L., Gräwe, U., Wilkin, J., & Fischer, J. (2023). Estimating the seasonal impact of optically significant water constituents on surface heating rates in the western Baltic Sea. *Biogeosciences*, 20(13), 2743-2768.
- Cazzaniga, I., Zibordi, G., & Mélin, F. (2021). Spectral variations of the remote sensing reflectance during coccolithophore blooms in the Western Black Sea. *Remote Sensing of Environment*, 264, 112607.
- Cazzaniga, I., & Zibordi, G. (2023). AERONET-OC LWN Uncertainties: Revisited. *Journal of Atmospheric and Oceanic Technology*, 40(4), 411-425.
- Cazzaniga, I., & Mélin, F. (2024). How Representative Are European AERONET-OC Sites of European Marine Waters?. *Remote Sensing*, 16(10), 1793.
- Cetinić, I., Rousseaux, C. S., Carroll, I. T., Chase, A. P., Kramer, S. J., Werdell, P. J., ... & Sayers, M. (2024). Phytoplankton composition from sPACE: Requirements, opportunities, and challenges. *Remote Sensing of Environment*, 302, 113964.
- Chami, M., Lafrance, B., Fougnie, B., Chowdhary, J., Harmel, T., & Waquet, F. (2015). OSOAA: a vector radiative transfer model of coupled atmosphere-ocean system for a rough sea surface application to the estimates of the directional variations of the water leaving reflectance to better process multi-angular satellite sensors data over the ocean. *Optics Express*, 23(21), 27829-27852.
- Cogliati, S., Sarti, F., Chiarantini, L., Cosi, M., Lorusso, R., Lopinto, E., ... & Colombo, R. (2021). The PRISMA imaging spectroscopy mission: overview and first performance analysis. *Remote sensing of environment*, 262, 112499.
- Concha, J. A., Bracaglia, M., & Brando, V. E. (2021). Assessing the influence of different validation protocols on Ocean Colour match-up analyses. *Remote Sensing of Environment*, 259, 112415.
- Coppo, P., Brandani, F., Faraci, M., Sarti, F., Dami, M., Chiarantini, L., ... & Cosi, M. (2020). Leonardo spaceborne infrared payloads for Earth observation: SLSTRs for Copernicus Sentinel 3 and PRISMA hyperspectral camera for PRISMA satellite. *Applied Optics*, 59(23), 6888-6901.
- Dierssen, H. M., Ackleson, S. G., Joyce, K. E., Hestir, E. L., Castagna, A., Lavender, S., & McManus, M. A. (2021). Living up to the hype of hyperspectral aquatic remote sensing: science, resources and outlook. *Frontiers in Environmental Science*, 9, 649528.
- Dogliotti, A. I., Piegari, E., Rubinstein, L., Perna, P., & Ruddick, K. G. (2024). Using the automated HYPERNETS hyperspectral system for multi-mission satellite ocean colour validation in the Río de la Plata, accounting for different spatial resolutions. *Frontiers in Remote Sensing*, 5, 1354662.
- Donlon, C., Berruti, B., Buongiorno, A., Ferreira, M. H., Féménias, P., Frerick, J., ... & Sciarra, R. (2012). The global monitoring for environment and security (GMES) sentinel-3 mission. *Remote sensing of Environment*, 120, 37-57.



<b>Project</b>	NECCON No 101081273	<b>Deliverable</b>	4.2
<b>Dissemination</b>	Public	<b>Nature</b>	Report
<b>Date</b>	31 <sup>st</sup> December 2024	<b>Version</b>	1.0

Doxaran, D., ElKilani, B., Corizzi, A., & Goyens, C. (2024). Validation of satellite-derived water-leaving reflectance in contrasted French coastal waters based on HYPERNETS field measurements. *Frontiers in Remote Sensing*, 4, 1290110.

Dutkiewicz, S., Hickman, A. E., Jahn, O., Gregg, W. W., Mouw, C. B., & Follows, M. J. (2015). Capturing optically important constituents and properties in a marine biogeochemical and ecosystem model. *Biogeosciences*, 12(14), 4447-4481.

European Union-Copernicus Marine Service. (2022). Mediterranean Sea, Bio-Geo-Chemical, L3, daily Satellite Observations (1997-ongoing) [Dataset]. Mercator Ocean International. <https://doi.org/10.48670/MOI-00299>

Giardino, C., Brando, V. E., Gege, P., Pinnel, N., Hochberg, E., Knaeps, E., ... & Dekker, A. (2019). Imaging spectrometry of inland and coastal waters: state of the art, achievements and perspectives. *Surveys in Geophysics*, 40, 401-429.

Giardino, C., Bresciani, M., Braga, F., Fabbretto, A., Ghirardi, N., Pepe, M., ... & Brando, V. E. (2020). First evaluation of PRISMA level 1 data for water applications. *Sensors*, 20(16), 4553.

Goetz, A. F., Vane, G., Solomon, J. E., & Rock, B. N. (1985). Imaging spectrometry for earth remote sensing. *science*, 228(4704), 1147-1153.

González Vilas, L. Brando, V.E. Concha, J.A., Goyens, C., Dogliotti, A.I., Doxaran, D., Dille, A., Van der Zande, D. (2024). Validation of satellite water products based on HYPERNETS *in situ* data using a Match-up Database (MDB) file structure. *Frontiers in Remote Sensing*, 5, 1330317.

Gordon, H. R., & Morel, A. Y. (2012). Remote assessment of ocean color for interpretation of satellite visible imagery: A review.

Gregg, W. W., & Rousseaux, C. S. (2016). Directional and spectral irradiance in ocean models: Effects on simulated global phytoplankton, nutrients, and primary production. *Frontiers in Marine Science*, 3, 240.

Gregg, W. W., & Rousseaux, C. S. (2017). Simulating PACE global ocean radiances. *Frontiers in Marine Science*, 4, 60.

Groom, S., Martinez-Vicente, V., Fishwick, J., Tilstone, G., Moore, G., Smyth, T., & Harbour, D. (2009). The western English Channel observatory: Optical characteristics of station L4. *Journal of Marine Systems*, 77(3), 278-295.

Guanter, L., Ruiz-Verdú, A., Odermatt, D., Giardino, C., Simis, S., Estellés, V., ... & Moreno, J. (2010). Atmospheric correction of ENVISAT/MERIS data over inland waters: Validation for European lakes. *Remote Sensing of Environment*, 114(3), 467-480.

Guanter, L., Kaufmann, H., Segl, K., Foerster, S., Rogass, C., Chabrillat, S., ... & Sang, B. (2015). The EnMAP spaceborne imaging spectroscopy mission for earth observation. *Remote Sensing*, 7(7), 8830-8857.

<b>Project</b>	NECCON No 101081273	<b>Deliverable</b>	4.2
<b>Dissemination</b>	Public	<b>Nature</b>	Report
<b>Date</b>	31 <sup>st</sup> December 2024	<b>Version</b>	1.0

- Holben, B. N., Eck, T. F., Slutsker, I. A., Tanré, D., Buis, J. P., Setzer, A., ... & Smirnov, A. (1998). AERONET—A federated instrument network and data archive for aerosol characterization. *Remote sensing of environment*, 66(1), 1-16.
- Ilori, C. O., Pahlevan, N., & Knudby, A. (2019). Analyzing performances of different atmospheric correction techniques for Landsat 8: Application for coastal remote sensing. *Remote Sensing*, 11(4), 469.
- Kruse, F. A., Lefkoff, A. B., Boardman, Y. J., Heidebrecht, K. B., Shapiro, A. T., Barloon, P. J., & Goetz, A. F. H. (1993). The spectral image processing system (SIPS)—interactive visualization and analysis of imaging spectrometer data. *Remote sensing of environment*, 44(2-3), 145-163.
- Kubryakov, A. A., Mikaelyan, A. S., & Stanichny, S. V. (2021). Extremely strong coccolithophore blooms in the Black Sea: The decisive role of winter vertical entrainment of deep water. *Deep Sea Research Part I: Oceanographic Research Papers*, 173, 103554.
- Kuusk, J., Corizzi, A., Doxaran, D., Duong, K., Flight, K., Kivastik, J., ... & Ruddick, K. (2024). HYPSTAR: a hyperspectral pointable system for terrestrial and aquatic radiometry. *Frontiers in Remote Sensing*, 5, 1347507.
- Lavigne, H., & Ruddick, K. (2021, July). Inter-band calibration for hyperspectral water remote sensing: demonstration for CHRIS-PROBA. In *2021 IEEE International Geoscience and Remote Sensing Symposium IGARSS* (pp. 7771-7774). IEEE.
- Lazzari, P., Salon, S., Terzić, E., Gregg, W. W., d'Ortenzio, F., Vellucci, V., ... & Antoine, D. (2021). Assessment of the spectral downward irradiance at the surface of the Mediterranean Sea using the radiative Ocean-Atmosphere Spectral Irradiance Model (OASIM). *Ocean Science*, 17(3), 675-697.
- Lazzari, P., Gharbi Dit Kacem, M., Álvarez, E., Chernov, I., & Vellucci, V. (2024). Determination of biogeochemical properties in sea waters using the inversion of the three-stream irradiance model. *Scientific Reports*, 14(1), 22347.
- Maggiorano, A., Baird, M., Langlais, C., Mongin, M., & Skerratt, J. (2024). Impact of phytoplankton, CDOM, and suspended sediments on the vertical attenuation of light, changing heat content and circulation on a continental shelf: A modelling study of the Great Barrier Reef. *Ocean Modelling*, 102465.
- Mediterranean Sea, Bio-Geo-Chemical, L3, daily Satellite Observations (1997-ongoing). E.U. Copernicus Marine Service Information (CMEMS). Marine Data Store (MDS). DOI: 10.48670/moi-00299 (Accessed on 29-11-2023)
- Mobley, C. D. (1999). Estimation of the remote-sensing reflectance from above-surface measurements. *Applied optics*, 38(36), 7442-7455.
- Morel, A., Antoine, D., & Gentili, B. (2002). Bidirectional reflectance of oceanic waters: accounting for Raman emission and varying particle scattering phase function. *Applied Optics*, 41(30), 6289-6306.

<b>Project</b>	NECCON No 101081273	<b>Deliverable</b>	4.2
<b>Dissemination</b>	Public	<b>Nature</b>	Report
<b>Date</b>	31 <sup>st</sup> December 2024	<b>Version</b>	1.0

NASA Ocean Biology Processing Group. (2024). PACE OCI Level-2 Surface Reflectance Data, V2.0 [Dataset]. NASA Ocean Biology Distributed Active Archive Center. DOI:10.5067/PACE/OCI/L2/SFREFL/2.0 (Accessed on 05/12/2024)

Pahlevan, N., Mangin, A., Balasubramanian, S. V., Smith, B., Alikas, K., Arai, K., ... & Warren, M. (2021). ACIX-Aqua: A global assessment of atmospheric correction methods for Landsat-8 and Sentinel-2 over lakes, rivers, and coastal waters. *Remote Sensing of Environment*, 258, 112366.

Park, Y. J., & Ruddick, K. (2005). Model of remote-sensing reflectance including bidirectional effects for case 1 and case 2 waters. *Applied Optics*, 44(7), 1236-1249.

Pellegrino, A., Fabbretto, A., Bresciani, M., de Lima, T. M. A., Braga, F., Pahlevan, N., ... & Giardino, C. (2023). Assessing the accuracy of PRISMA standard reflectance products in globally distributed aquatic sites. *Remote Sensing*, 15(8), 2163.

Rast, M., & Painter, T. H. (2019). Earth observation imaging spectroscopy for terrestrial systems: An overview of its history, techniques, and applications of its missions. *Surveys in Geophysics*, 40(3), 303-331.

Ruddick, K. G., Brando, V. E., Corizzi, A., Dogliotti, A. I., Doxaran, D., Goyens, C., ... & Van der Zande, D. (2024a). WATERHYPERNET: a prototype network of automated *in situ* measurements of hyperspectral water reflectance for satellite validation and water quality monitoring. *Frontiers in Remote Sensing*, 5, 1347520.

Ruddick, K. G., Bialek, A., Brando, V. E., De Vis, P., Dogliotti, A. I., Doxaran, D., ... & Vanhellemont, Q. (2024b). HYPERNETS: a network of automated hyperspectral radiometers to validate water and land surface reflectance (380–1680 nm) from all satellite missions. *Frontiers in Remote Sensing*, 5, 1372085.

Sciuto, P., Mélin, F., Cazzaniga, I. and Bulgarelli, B. (2024) Reference measurements from AERONET-OC to assess Earth Observation data, Publications Office of the European Union, Luxembourg, 2024, doi:10.2760/245775, JRC136578.

Skakala, J., Bruggeman, J., Brewin, R. J., Ford, D. A., & Ciavatta, S. (2020). Improved representation of underwater light field and its impact on ecosystem dynamics: A study in the North Sea. *Journal of Geophysical Research: Oceans*, 125(7), e2020JC016122.

Skákala, J., Bruggeman, J., Ford, D., Wakelin, S., Akpınar, A., Hull, T., ... & Ciavatta, S. (2022). The impact of ocean biogeochemistry on physics and its consequences for modelling shelf seas. *Ocean Modelling*, 172, 101976.

Smyth, T. J., Fishwick, J. R., Gallienne, C. P., Stephens, J. A., & Bale, A. J. (2010). Technology, design, and operation of an autonomous buoy system in the western English Channel. *Journal of Atmospheric and Oceanic Technology*, 27(12), 2056-2064.

<b>Project</b>	NECCON No 101081273	<b>Deliverable</b>	4.2
<b>Dissemination</b>	Public	<b>Nature</b>	Report
<b>Date</b>	31 <sup>st</sup> December 2024	<b>Version</b>	1.0

Soppa, M. A., Brell, M., Chabrillat, S., Alvarado, L. M., Gege, P., Plattner, S., ... & Bracher, A. (2024). Full mission evaluation of EnMAP water leaving reflectance products using three atmospheric correction processors. *Optics Express*, 32(16), 28215-28230.

Steinmetz, F., Deschamps, P. Y., & Ramon, D. (2011). Atmospheric correction in presence of sun glint: application to MERIS. *Optics express*, 19(10), 9783-9800.

Steinmetz, F., & Ramon, D. (2018, October). Sentinel-2 MSI and Sentinel-3 OLCI consistent ocean colour products using POLYMER. In *Remote sensing of the open and coastal ocean and inland waters* (Vol. 10778, pp. 46-55). SPIE.

Thuillier, G., Hersé, M., Labs, D., Foujols, T., Peetermans, W., Gillotay, D., ... & Mandel, H. (2003). The solar spectral irradiance from 200 to 2400 nm as measured by the SOLSPEC spectrometer from the ATLAS and EURECA missions. *Solar Physics*, 214, 1-22.

Transon, J., d'Andrimont, R., Maignard, A., & Defourny, P. (2018). Survey of hyperspectral earth observation applications from space in the sentinel-2 context. *Remote Sensing*, 10(2), 157.

Valente, A., Sathyendranath, S., Brotas, V., Groom, S., Grant, M., Taberner, M., ... & Zibordi, G. (2016). A compilation of global bio-optical *in situ* data for ocean-colour satellite applications. *Earth System Science Data*, 8(1), 235-252.

Vanhellemont, Q., & Ruddick, K. (2014). Turbid wakes associated with offshore wind turbines observed with Landsat 8. *Remote Sensing of Environment*, 145, 105-115.

Vanhellemont, Q., & Ruddick, K. (2016, May). Acolite for Sentinel-2: Aquatic applications of MSI imagery. In *Proceedings of the 2016 ESA Living Planet Symposium, Prague, Czech Republic* (Vol. 9).

Vanhellemont, Q. (2019). Adaptation of the dark spectrum fitting atmospheric correction for aquatic applications of the Landsat and Sentinel-2 archives. *Remote Sensing of Environment*, 225, 175-192.

Vanhellemont, Q. (2020). Sensitivity analysis of the dark spectrum fitting atmospheric correction for metre-and decametre-scale satellite imagery using autonomous hyperspectral radiometry. *Optics Express*, 28(20), 29948-29965.

Vanhellemont, Q., & Ruddick, K. (2021). Atmospheric correction of Sentinel-3/OLCI data for mapping of suspended particulate matter and chlorophyll-a concentration in Belgian turbid coastal waters. *Remote Sensing of Environment*, 256, 112284.

Vansteenkewegen, D., Ruddick, K., Cattrijsse, A., Vanhellemont, Q., & Beck, M. (2019). The pan-and-tilt hyperspectral radiometer system (PANTHYR) for autonomous satellite validation measurements—Prototype design and testing. *Remote Sensing*, 11(11), 1360.

Warren, M. A., Simis, S. G., Martinez-Vicente, V., Poser, K., Bresciani, M., Alikas, K., ... & Ansper, A. (2019). Assessment of atmospheric correction algorithms for the Sentinel-2A MultiSpectral Imager over coastal and inland waters. *Remote sensing of environment*, 225, 267-289.

<b>Project</b>	NECCTON No 101081273	<b>Deliverable</b>	4.2
<b>Dissemination</b>	Public	<b>Nature</b>	Report
<b>Date</b>	31 <sup>st</sup> December 2024	<b>Version</b>	1.0

Werdell, P. J., Behrenfeld, M. J., Bontempi, P. S., Boss, E., Cairns, B., Davis, G. T., ... & Remer, L. A. (2019). The plankton, aerosol, cloud, ocean ecosystem mission: Status, science, advances. *Bulletin of the American Meteorological Society*, 100(9), 1775-1794.

Zibordi, G., Berthon, J. F., Bulgarelli, B., D'alimonte, D., Linde, D. V. D., Mélin, F., & Targa, C. (2004). Ocean colour validation activities at the Acqua Alta Oceanographic Tower in the northern Adriatic Sea. *International Journal of Remote Sensing*, 25(7-8), 1533-1537.

Zibordi, G., Mélin, F., & Berthon, J. F. (2006). Comparison of SeaWiFS, MODIS and MERIS radiometric products at a coastal site. *Geophysical Research Letters*, 33(6).

Zibordi, G., Berthon, J. F., Mélin, F., D'Alimonte, D., & Kaitala, S. (2009a). Validation of satellite ocean color primary products at optically complex coastal sites: Northern Adriatic Sea, Northern Baltic Proper and Gulf of Finland. *Remote Sensing of Environment*, 113(12), 2574-2591.

Zibordi, G., Mélin, F., Berthon, J.F., Holben, B., Slutsker, I., Giles, D., D'Alimonte, D., Vandemark, D., Feng, H., Schuster, G., Fabbri, B.E., Kaitale, S., & Seppälä, J., (2009b). AERONET-OC: A Network for the Validation of Ocean Color Primary Products. *Journal of Atmospheric and Oceanic Technology*, 26, 1634-1651.

Zibordi, G., Holben, B., Mélin, F., D'Alimonte, D., Berthon, J. F., Slutsker, I., & Giles, D. (2010). AERONET-OC: an overview. *Canadian Journal of Remote Sensing*, 36(5), 488-497.

Zibordi, G., Holben, B. N., Talone, M., D'Alimonte, D., Slutsker, I., Giles, D. M., & Sorokin, M. G. (2021). Advances in the ocean color component of the aerosol robotic network (AERONET-OC). *Journal of Atmospheric and Oceanic Technology*, 38(4), 725-746.

Zibordi, G., Kwiatkowska, E., Mélin, F., Talone, M., Cazzaniga, I., Dessailly, D., & Gossn, J. I. (2022). Assessment of OLCI-A and OLCI-B radiometric data products across European seas. *Remote Sensing of Environment*, 272, 112911.